Elsevier Editorial System(tm) for Corrosion Science

Manuscript Draft

Manuscript Number:

Title: Influence of mortar resistivity on the rate-limiting step of chloride-induced macro-cell corrosion of reinforcing steel

Article Type: Full Length Article

Keywords: A - steel reinforced concrete, concrete
C - pitting corrosion

Corresponding Author: Mrs. Karla Hornbostel,

Corresponding Author's Institution: Norwegian University of Science and Technology

First Author: Karla Hornbostel

Order of Authors: Karla Hornbostel; Ueli M. Angst; Bernhard Elsener; Claus K. Larsen; Mette R. Geiker

Abstract: The influence of mortar resistivity on the kinetics of chloride-induced macro-cell corrosion of the reinforcement was experimentally studied. It was found that the corrosion process was limited by a combination of anodic, ohmic and cathodic control for the geometrical conditions tested (small anodes, large cathode-to-anode ratio). The cathodic partial process was independent of the bulk resistivity. Both the anodic and the ohmic partial processes were influenced by local conditions around the anode but were not directly related to the bulk resistivity. The findings indicate that a unique relationship cannot exist between bulk resistivity and the corrosion rate for macro-cell corrosion.

Cover Letter

Karla Hornbostel
NTNU Department of Structural Engineering
Richard Birkelandsvei1a
7491Trondheim
Norway

Trondheim August 26, 2015

Dear editors of Corrosion Science,

Attached you find a manuscript entitled:

Influence of mortar resistivity on the rate-limiting step of chloride-induced macro-cell corrosion of reinforcing steel,

authored by

Hornbostel, Karla; Angst, Ueli M.; Elsener, Bernhard; Larsen, Claus K. and Geiker, Mette R.

The influence of mortar resistivity on the kinetics of chloride-induced macro-cell corrosion of the reinforcement was experimentally studied. It was found that the corrosion process was limited by a combination of anodic, ohmic and cathodic control for the geometrical conditions tested (small anodes, large cathode-to-anode ratio). The cathodic partial process was independent of the bulk resistivity. Both the anodic and the ohmic partial processes were influenced by local conditions around the anode but were not directly related to the bulk resistivity. The findings indicate that a unique relationship cannot exist between bulk resistivity and the corrosion rate for macro-cell corrosion.
The paper is based on work carried out at the NTNU Trondheim and within the COIN project. It was supported by the Norwegian Public Roads Administration.

I hope you find the paper appropriated for publishing in your journal.

Best regards

Karla Hornbostel

Highlights

- A unique correlation between concrete bulk resistivity and the corrosion rate frequently claimed in the literature cannot exist for chloride induced macro-cell corrosion as the partial processes underlying corrosion propagation cannot directly be related to the bulk concrete resistivity.

- The results presented in the study clearly indicate that the anodic partial process is influenced primarily by the local conditions around the anode rather than by the bulk resistivity for the anode size tested (small anodes). It appears that mass transfer limitations govern the anodic reaction, the concept of anodic resistance was found adequate to describe this observation.

- The reaction kinetics of the cathodic partial process (oxygen reduction) were found to be practically independent on the mortar bulk resistivity.

- Ohmic resistance arising in the concrete in the direct vicinity of the anode dominates the ohmic partial process for laboratory-scale mortar specimens. The resistance is strongly influenced by local conditions and is therefore, especially for small anodes not directly correlated to the bulk concrete resistivity.

Influenceof mortar resistivity on the rate-limiting step of chloride-induced macro-cell corrosion of reinforcing steel

Hornbostel,Karla[a*]; Angst, Ueli M.[b,c]; Elsener,Bernhard[b,d]; Larsen, Claus K.[a,e] and Geiker, Mette R.[a]

[a] Norwegian University of Science and Technology, Department of Structural Engineering, Richard Birkelandsvei 1a, 7491 Trondheim, Norway

[b] ETH Zurich, Institute for Building Materials (IfB), Stefano-Franscini-Platz 3, 8093 Zurich, Switzerland

[c]Swiss Society for Corrosion Protection (SGK), Technoparkstrasse 1, 8005 Zurich, Switzerland

[d]University of Cagliari, Department of Chemical and Geological Science, 09100 Monserrato (CA), Italy

[e]Norwegian Public Roads Administration, Brynsengfaret 6A, 0667 Oslo, Norway

* Corresponding author: Richard Birkelandsvei 1a, 7491 Trondheim, Norway, +47 73594537, Karla.Hornbostel@ntnu.no

Abstract

The influence of mortar resistivity on the kinetics of chloride-induced macro-cell corrosion of the reinforcement was experimentally studied. It was found that the corrosion process waslimited by a combination of anodic, ohmic and cathodic controlfor the geometrical conditions tested (small anodes, large cathode-to-anode ratio). The cathodic partial process was independent of the bulk resistivity. Both the anodic and the ohmic partial processeswere influenced by local conditions around the anode but were not directly related to the bulk resistivity. The findings indicate that a unique relationship cannotexist between bulk resistivity and the corrosion rate for macro-cell corrosion.

Key words

A – steel reinforced concrete, concrete

C – pitting corrosion

1 Introduction

Whenreinforced concrete structures are exposed to sea water or chloride-contaminated surface water (e.g. from de-icing salts),chlorides penetrate the concrete cover and initiate corrosion when a critical concentration is exceeded at the reinforcement[1]. Local pits (anodes) that formon the steel arevery small compared to the size of the uncorroded steel area (cathode). In the corrosion process,anode and cathode are spatially separated, and their galvanic interaction is termed ‘macro-cell corrosion’. The electrochemical mechanism of the corrosion process is illustrated in Figure 1.The anodic partial process describes the dissolution of iron. During the release of ferrous ions into the electrolyte, electrons are left behind in the metallic phase and transported to cathodic areas ofthe steel surface,where they are consumed in a cathodic reaction (cathodic partial process). To maintain charge balance between the anodic and cathodic processesan ionic macro-cell current flow is established from the anode to the cathode in the electrolyte (ohmic partial process) andthe partial processes have to procedd at the same rate. [2]

In the literature, variousfactors are indentifiedthat influencethese partial processes and thus the corrosion rate; among others,the moisture content, temperature, concrete composition, and the geometry of the macro-cellwere found decisive[4-14]. The overall rate of the corrosion process is commonly assumed to be limited by the slowest of the partial processes. Cathodic control was found in both experimentsand numerical modelling in studies investigating macro-cell arrangements with relatively large anodes [4, 9, 12]. Anodic control was observed for chloride-induced localized corrosion in experiments analysing potential changesin the early and intermediate stages of corrosion propagation, i.e.for presumably smaller anodes[8, 10, 11]. These last three studies also introduced the concept of ‘anodicresistance control’ to

describe the indirect influence of concrete resistivity on the anodic partial process,limiting ion transport to the anode.

In the literature, a trend of decreasing corrosion rate with increasing concrete resistivity is generally reported.However, the variation and scatter in the correlation data both within and between the various studies is high and not well explained [15]. Ohmic andanodicresistance control of the corrosion process would suggest a certain influence of concrete resistivity on the corrosion process.

The aim of the present study was to investigate the influence of concrete resistivity on the individual partial processes and toprovide an improved mechanistic understanding of the corrosion rate-limiting steps. An experimental setup was used with small pieces of mild steel (simulated anodes) placed in a network of stainless steel tubes and bars (cathodes) embedded in different mortar specimens exposed to chlorides. The simulated anodes used in the experiment were intended to represent pitslocated in an otherwise passive and well-aerated cathode network.

2Experimental

2.1 Experimental setup

The experimental setup is shown in Figure 2. The simulated anodes were produced from a smooth mild steel bar (S235JR Ø 6 mm) cut into 5-6 mm long pieces. Each piece was sandblasted and coated with heat-shrink tubing leaving justone cut surface uncovered (exposed area 28.3 mm^2). To avoid crevice corrosion between the steel pieces and the heat-shrink tubing, a coating of abrasion-resistant, very dense cement paste (Portland cement and Febond SBR, in volumeproportion 1.2:1) was applied around the lateral surface of the steel pieces. To increase the probability of corrosion onset, four simulated anodes were mounted on

one stainless steel tube (denoted C1, AISI 316 Ø 12 mm, exposed area 4270 mm^2). The simulated anodes wereall mountedon the same side of the tube with a centre-to-centre distance of 20 mm(cf. Figure 2, 'instrumented tube'). After mounting thesimulated anodes, the instrumented tube was filled with acryl.All the steel elements were electrically insulated; connections between them could be established manually.

In addition to the instrumented tube, four stainless steel bars (denoted C1-1, C1-2, C2-1, C2-2, AISI 316L Ø 10 mm, exposed area per bar 3770 mm^2) were placed at different distances from the simulated anodes(Figure 2). The stainless steel tube and the stainless steel bars were preheated toa temperature of 700 °C for 10 minutes, with subsequent cooling in cold tap water. The oxide scale formed on the surface of the stainless steelas a result ofthis treatment increased the exchange current density of the cathodic reaction to levels comparable with normal carbon steel [16-18].

Amanganese dioxide reference electrode (ERE 20, FORCE TECHNOLOGY) was embedded in each mortar specimen. A metal mesh was used as a counter electrode. Six resistivity sensorswere also embedded in each specimen,but the measurements undertaken with the sensors are not presented in this paper.

2.2 Materials and exposure

Two mortar mixes with different bulk resistivity were prepared (Table 2). The low-resistivity mortar(*PC*) had a water/binder ratio (*w/b*) of 0.55 and was made from Portland cement (CEM I 42.5 R). The high-resistivity mortar (*FA*) was prepared with a low *w/b* ratio of 0.40 and 30% of the Portland cement was replaced by fly ash. The casting direction is indicated inFigure 2,

the simulated anodes were placed facing the lower,chloride-exposed surface.Atotal of nine specimens were cast per mix. Exposure conditions and specimen IDsare given in Table 3.

All mortar specimens were wrapped in plastic foil after demoulding, 24 hours after casting. The specimens were cured sealed for several weeks (four weeks for PC specimens and 18 weeks for FA specimens) in a climate chamber with a constant temperature of 20 °C. After curing, the sides and the top face of all mortar specimens were epoxy-coated to ensure one-dimensional moisture and chloride profiles. Subsequently, the initial mortar cover to the simulated anodes was reduced from 30 mm to 10 mm by cutting (cf. Figure 2). This was done to limit the wall effect and at the same time facilitate rapid corrosion initiation [19, 20]. To further facilitate ingress of water and chlorides, the specimens were stored in an oven at 30 °C (RH ~25%) for partial drying [20] prior to exposure to the chloride solution (3M sodium chloride (NaCl)). After corrosion onset, the exposure conditions were varied, see Table 3. It should be noted that the FA and PC specimens were treated differently.

2.3 Methods of investigation

Before corrosion onset, all simulated anodes were connected with the cathode network. Once corrosion initiation was detected (by potential measurements), the simulated anode which first showed signs of active corrosion in each specimen was identified. The other simulated anodes were disconnected from the cathode network, and no further investigations of them are reported in this paper. The measurements presented here were undertaken for the macro-cell arrangement where the simulated anode in each specimen was connected with all the cathodes: C1, C1-1, C1-2, C2-1, C2-2 (cf. Figure 2). The cathode-to-anode ratio was 685.

2.3.1 Ohmic resistance

The bulk resistivity of the mortar (ρ_{bulk}) at the level of the simulated anode was determined by measuring the resistance between the stainless steel bar (C1-2) and the instrumented tube (C1) and applying a pre-calibrated cell constant.

The ohmic resistance between the simulated anode and the entire cathode network was also measured. The area ratio between cathode and anode is extremely large, so it can be reasonably assumed that this resistance is a close approximation of the spreading resistance (bottle neck effect) of the anode, this was also shown in [21]. In present paper, the resistance measured between the anode and the cathode is termed $R_{\Omega,a}$.

Bulk resistance measurements were carried out using an LCR meter (frequency 1 kHz, square pulse ca. 0.9 V). All other resistance measurements were made with electrical impedance spectroscopy (EIS), using a potentiostat of the type Princeton Applied Research Parstat 2273. The EIS was performed in a frequency range between 500 kHz and 1 Hz. The AC amplitude was adjusted to the mortar specimen tested; in most cases, 10 mV was chosen for the PC specimens and 40 mV for the FA specimens. The ohmic resistance was determined as the impedance with the minimum phase angle in the chosen frequency range.

2.3.2 Galvanic current

The galvanic current (I_{galv}) between the simulated anode and the cathode network was measured using zero-resistance ammeters. The measurements were made using either the data logger system Camur II from Protector (ZRA-node) or the potentiostat. The data measured with the two devices were comparable. During most of the period of investigation, the

galvanic current was measured at least once a day. Only data indicating active corrosion (galvanic currents > 0.1 μA) are presented here.

2.3.3 Polarization curves

Electrochemical potentials were measured against the manganese dioxide reference electrode embedded in each specimen. The potential of the reference electrode versus an external saturated calomel reference electrode (SCE) was provided by the manufacturer and randomly checked before and after casting. Measurements of potentials are presented versus SCE.

Anodic and cathodic polarization curves were measured by taking a potentiodynamic polarization scan using the potentiostat. The measurements were made at least 12 hours after disconnecting the simulated anode and the cathode network from each other. The cathodic polarization curves were measured with all the cathodes connected. They therefore represent an average of the cathodes located at two different depths (cf. Figure 2, cathode C1, C1-x and C2-x). The curves were recorded from the open circuit potential until a potential of approximately -470 mV vs. SCE with a scan rate of 0.1667 mV/s and a step height of 5 mV. The anodic polarization curves of the simulated anodes were started from the open circuit potential of the simulated anode with a scan rate of 0.1 mV/s and a step height of 5 mV until a potential of approximately -70 mV vs. SCE was reached. In all cases, the scans were done with automatic IR compensation of the potentiostat (current interruption method). The correctness of the IR compensation was randomly checked by separate ohmic drop measurements with EIS as proposed by [22].

2.3.4 Opening of the mortar specimens

Selected mortar specimens were opened after all tests were completed. The condition of the simulated anodes and the surrounding mortar was examined (examples of 3D scans of cleaned corroded anodes are shown in Figure 3).

The volume loss from the simulated anodes was determined using 3D scanning (details are provided in [17]) and on the basis of galvanic current measurements. The latter were made using Faraday's law [2]:

$$V_{theo} = \frac{Q \cdot M}{F \cdot z} \frac{1}{\rho} \quad (1)$$

where Q is the charge passed, M the molar mass of steel (56 g/mol), F the Faraday constant (96485 C/mol), z the number of electrons transferred per ion (here 2), and ρ the steel density (7.874 g/cm^3). The results of the volume loss calculations are compared in Table 4. The amount of micro-cell corrosion was calculated as the difference between the volume loss from 3D scanning and that calculated from the galvanic current measurements. It should be noted that both methods are subject to uncertainties and the results are only indicative.

3 Results

3.1 Galvanic current measurements and microcell corrosion

Although the simulated anodes were chosen to be small in size, a certain extent of micro-cell corrosion could not be avoided. Comparison between the volume loss calculated from 3D scanning and that calculated from galvanic current measurements indicates a substantial amount of self-corrosion especially for the FA specimens (cf. Table 4). This means that the galvanic current measured for the FA specimens does not account for the total corrosion

current. For the PC specimens, on the other hand, the extent of micro-cell corrosion seems to be negligible, and it can therefore be assumed that the galvanic current gives a reasonable approximation of the actual corrosion current.

Table 4 also shows that the corrosion had propagated considerably more for the PC specimens with a volume loss of up to 10 times higher than that found for the FA specimens. This marked difference is most likely a combined effect of the different curing times and exposure conditions (cf. Table 3) as well as the different material properties (cf. Table 2).

3.2 Resistance measurements

The resistance measured between the simulated anodes and the cathode network ($R_{\Omega,a}$) was compared with the bulk resistivity (Figure 4). As expected, a trend can be found in the results. However, a considerable scatter is observed in the data as well. For a given bulk resistivity, $R_{\Omega,a}$ differs by as much as one order of magnitude.

3.3 Polarization curves

Anodic and cathodic polarization curves were measured occasionally during the testing period. The curve examples shown in Figure 5 are representative for other specimens and points in time.

3.3.1 Cathodic polarization curves

Figure 5 a) shows an exponential law for the cathodic polarization curve, indicating that the reaction kinetics were activation-controlled. In an E-log I diagram (Figure 5 b)), the cathodic polarization curve becomes a straight line and can be expressed by a Tafel equation [23]:

$$E_c - E_c^{rev} = \beta_c \log\left|\frac{I_c}{I_c^o}\right| \quad (2)$$

The slope of the curve is termed the cathodic Tafel constant (β_c) and the current extrapolated to the reversible potential is the exchange current I_c^o (Figure 5 b)). Figure 6 shows the cathodic Tafel constant and the exchange current as a function of bulk resistivity for the specific specimen at the time of measuring the polarization curve. Note that in this research, the cathode was preheated stainless steel, which is not directly comparable with common carbon steel. Nevertheless, the Tafel constants obtained (between 100 and 300 mV/dec) are in good agreement with results for carbon steel (between 100 and 240 mV/dec in the literature, [8, 9, 12, 24]). Moreover, the exchange current densities identified (0.6 – 5.0 10^{-2}μA/cm^2) are in the same range as data reported in the literature ($1.2\cdot10^{-2}$ – $1.5\cdot10^{-1}$μA/cm^2, [9, 12, 25]).

In Figure 6, no correlation can be observed between the bulk resistivity and the cathodic Tafel constant or the cathodic exchange current. The data is randomly distributed within the resistivity range of each of the two different materials. While the cathodic Tafel constant is somewhat more variable in the PC specimens, the mean value is comparable (~0.2 V/dec) with that of the FA specimens. The exchange current density is lower in the FA than in the PC specimens.

3.3.2 Anodic polarization cures

The anodic polarization curves are linear in the E-I diagram (Figure 5 a)) and consequently do not exhibit Tafel behaviour in the E-log I diagram (Figure 5 b)). In the range tested, the polarization behaviour can be expressed in the form of a simple anodic polarization resistance, R_{pa}:

$$R_{pa} = \frac{E_a - E_a{}^{rev}}{I_a} \quad (3)$$

There is very little in the literature about anodic polarization curves of locally corroding steel in concrete. The reports available from other researchers indicate comparable observations ([25] and the literature cited therein).

Figure 7 shows R_{pa} as a function of the bulk resistivity and of $R_{\Omega,a}$(Figure 7 a) and b)). The values obtained for R_{pa} are in good agreement with the literature, (0.13 -1.4 Ωm^2, [26, 27]). Some higher values (0.5-2 Ωm^2, [25]) are also reported, but there comparatively large anodes were tested.

Figure 7 a) shows that there is no explicit correlation between R_{pa} and the bulk resistivity. However, it is noticeable that R_{pa} measured in FA tends to be higher than R_{pa} measured in PC. When these polarization resistances are compared with $R_{\Omega,a}$rather than with the bulk resistivity, a trend is revealed (Figure 7 b)).

It should be noted that the anodic polarization curves were IR compensated, so the values derived for R_{pa} do not include the IR drop in the mortar during polarization. It is therefore unlikely that the correlation between $R_{\Omega,a}$ and R_{pa} can be explained by a dominating influence of $R_{\Omega,a}$ on the polarization measurements performed. However, we are well aware of the experimental difficulties associated with compensating for the IR drop in such measurements, particularly in the case of high ohmic resistances as in the present case with small working electrodes (simulated anodes) and distant reference electrodes. Nevertheless, a number of different approaches used to compensate for the IR drop in this research indicated that the sort

of polarization curves shown in Figure 5 are indeed good approximations of IR-free polarization curves.

3.4 Galvanic current and bulk resistivity/ cell resistance

In Figure 8 a), the bulk resistivity is compared with the galvanic current measured between the simulated anodes and the cathode network. A trend of decreasing galvaniccurrent with increasing mortar resistivity can be observed. The data sets for the two materials tested are clearly separated from another. It should be noted that the galvanic current underestimates the actual corrosion current for the FA specimens; this is indicated in the figure by a dashed grey-line (assuming a self-corrosion fraction of 50%). Consequently, if self-corrosion had been taken into account, the trends for the data of the two materials would been even more separated. The scatter within the data sets is high. These observations reflect findings reported in the literature [15].

In Figure 8 b), where the galvanic current is compared with $R_{\Omega,a}$ (rather than with the bulk resistivity), the trends for the two materials draw closer together. However, due to the large amount of micro-cell corrosion observed on anodes in the FA specimens, the trends here too would probably be more separated if the actual corrosion currents had been taken into account (this is indicated by a grey dashed line in Figure 8 b)). Nevertheless, the overall trend and correlation to the galvanic current is more distinct for $R_{\Omega,a}$ than for the bulk resistivity. This is in agreement with what has already been observed for the polarization resistance of the simulated anodes (cf. Figure 7 b)).

4 Discussion

4.1 A conceptual model for the relevant steps that contribute to macro-cell corrosion

The corrosion process (cf. Figure 1) may be illustrated with the help of equivalent circuits [12, 25, 28] where, as a simplification, all the partial processes are represented by pure ohmic resistors connected in series, apart from the cathode, which is subdivided into segments connected in parallel(Figure 9).

The anodic and cathodic charge transfer reactions, i.e. the electrochemical oxidation and reduction reactions that occur at the steel/concrete interfaces, are represented by charge transfer resistances, $R_{ct,a}$ and $R_{ct,c,i}$. Due to the specific geometrical situation of localized or pitting corrosion, the ohmic partial process is subdivided into a part associated with the anode ($R_{\Omega,a}$), introduced earlier as the spreading resistance of the anode, and a number of resistances associated with individual cathode segments ($R_{\Omega,c,i}$).

Considering the cathode as a parallel circuit of a number of cathodic segments, each consisting of a charge transfer resistance $R_{ct,c,i}$and ohmic resistance $R_{\Omega,c,i}$ in series, allows us to distinguish properly between the kinetics related to the cathodic reaction and the influence of the ohmic resistance. Since $R_{\Omega,c,i}$ is related to charge transport between the anode and cathode segment *i*, it must be considered a part of the ohmic partial process and not part of the cathodic. The influence and magnitude of $R_{\Omega,c,i}$will depend mainly on the bulk resistivity of the concrete and the distance of the individual cathode segments from the anode. For remote cathode segments, $R_{\Omega,c,i}$ will be high and eventually exceed the charge transfer resistance $R_{ct,c,i}$. For typical laboratory specimens with small dimensions, there are no such remote cathode segments (cf.Figure 9) and consequently the $R_{\Omega,c,i}$ of all segments acting in the macro-cell is low. Moreover, due to the marked size ratio of anode and cathode in pitting

corrosion, the ohmic resistance of the anode ($R_{\Omega,a}$) was found to be much higher than that of the cathode when small anodes are considered due to the concentration of current (bottle neck effect) in front of small anodes, cf. [21]. Consequently, the cathodic part of the ohmic partial process ($R_{\Omega,c,i}$) might be negligible here. In large-scale structures, however, the ohmic resistance of remote cathode segments ($R_{\Omega,c,i}$) can limit the accessible cathode area, and this ohmic resistance might therefore be one of the dominating rate-limiting steps as will be discussed in a later section of the present paper (cf. Section 4.4).

In the conceptual approach introduced here (Figure 9), the anodic part of the ohmic partial process ($R_{\Omega,a}$) is essentially a part of the ohmic partial process. However, for the concept of anodic resistance control [8, 10, 11], a combined influence is assumed, comprising the charge transfer resistance and the ohmic resistance of the anode (i.e. anodic resistance control = $R_{ct,a}$ + $R_{\Omega,a}$, cf. the diagonal hatching inFigure 9).

4.2 Influence of mortar resistivity on the partial processes

4.2.1 Ohmic partial process

The ohmic partial process can be considered as consisting of two parts (cf. Figure 9):

- the current flow through the ohmic resistance associated with the anode $R_{\Omega,a}$ (the spreading resistance of the anode),

and

- the current flow through the ohmic resistance associated with the cathodes $R_{\Omega,c,i}$. (In the case of small-scale laboratory experiments, as here, with a high ratio between cathode and anode, this is considered negligible, cf. Section 4.1).

An investigation of the anodic part of the ohmic partial process ($R_{\Omega,a}$) has been presented in a recent publication by the present authors [21]. A considerable scatter was found between the bulk resistivity and $R_{\Omega,a}$ (the resistance between small simulated anodes (of the same size as tested here) and a cathode network). The large variations were ascribed to inhomogeneities such as aggregates, voids and other defects in the near vicinity of the simulated anodes and of the same size. A similar scatter was found in the present study (cf. Figure 4), namely that $R_{\Omega,a}$can vary by up to one order of magnitude for a given bulk resistivity. This indicates that $R_{\Omega,a}$cannot be directly predicted from bulk resistivity measurements for 'small' anode sizes, where 'small' means dimensions of the anode below or equal to those of mortar inhomogeneities such as aggregates and voids. Anodes typical of the early (and intermediate) phases in the propagation of chloride-induced corrosion in mortar are of this size.

As the anode size increases, reaching and exceeding the dimensions of voids and aggregates in concrete, the variation decreases and eventually vanishes. For simulated anodes with dimensions far beyond the maximum aggregate size, no influence of inhomogeneities was observed [25, 29]. Consequently, the extent to which variation in cell resistance needs to be taken into account in service life modelling depends mainly on the assumed anode size.

4.2.2 Cathodic partial process

As can be seen from Figure 6, there is no clear effect of bulk resistivity on the Tafel constant or the exchange current. However, the exchange current density is influenced by the type of mortar (cf. Figure 6 b)). The current density that the cathode can provide is smaller in the FA mortars than in the PC mortars. This difference in the level of cathodic current capacity may be explained by differences in the pore solution chemistry (lower OH^- concentration), which is a well-known factor affecting the exchange current density of the oxygen reduction reaction

[30]. Another likely explanation is that the effective steel surface area available for electrochemical reactions is lower in the FA mortar than in the PC mortar due to the denser mortar matrix giving a higher coverage of the steel surface with cement hydration products. Although these factors (pore solution chemistry, mortar matrix) may also be reflected in mortar resistivity, Figure 6 does not provide a basis for adequately expressing the cathodic reaction kinetics as a function of mortar resistivity alone. The fact that the cathodic reaction kinetics (Tafel slope and exchange current density) cannot be directly related to the concrete resistivity is also apparent from the well-known situation of low corrosion rates at low concrete resistivity in water-saturated concrete [2].

Consequently, in situations where the cathodic partial process dominates the corrosion process, no correlation between corrosion rate and mortar resistivity can be expected.

4.2.3 Anodic partial process

As can be seen from Figure 7 a), there is no direct correlation between bulk resistivity and the polarization resistance of the anodes (R_{pa}) across all the results obtained. The data is randomly distributed for the PC specimens; for the FA specimens a trend can be observed for increasing R_{pa} with increasing mortar resistivity. However, the data sets for the two mortar mixes are clearly separated. The R_{pa} for anodes embedded in PC specimens is somewhat lower than for those in FA specimens. This indicates that the anodic reaction can proceed at a higher rate in the PC specimens than in the FA specimens.

Comparison between R_{pa} and $R_{\Omega,a}$, (cf. Figure 7 b)) reveals that the data sets from the two materials tested overlap, with a trend of increasing polarization resistance with increasing $R_{\Omega,a}$. This implies that the anodic partial reaction is directly influenced by the local conditions

in the vicinity of the anode, namely the spreading resistance of the anode. This suggests that R_{pa} is governed by mass transfer control, i.e. that the current, which the anode provides at a certain applied potential, is determined by the flow of ionic species towards the anode (e.g. chloride) and away from the anode (primarily ferrous ions). Because this flow of ionic current has to occur through the pore system of the concrete in the vicinity of the anode (bottle neck effect), this mass transport limitation probably controls the anodic charge transfer reaction on the steel surface. The extent to which such anodic mass transfer limitations can occur seems related to the electrical resistance, i.e. to $R_{\Omega,a}$.

This mechanism of anodic mass transfer control has been hypothesized in earlier studies [5, 10, 11], and the term 'anodic resistance control' has been proposed. The special experimental setup in the present research permitted separation of the effects by plotting the relationship shown in Figure 7 b). This is strong evidence for the hypothesis of 'anodic resistance control', which is considered an appropriate term for the process. There is still a scatter in the correlation between R_{pa} and $R_{\Omega,a}$, which may be explained by differences in the local pH in pits and in their chloride content. Uncertainties are also related to the effective anodic area.

In summary, the present results clearly indicate that the anodic partial process is influenced primarily by the local conditions around the anode rather than by the bulk resistivity. It appears that mass transfer limitations govern the anodic reaction.

4.3 Quantifying the rate-limiting step of chloride-induced macro-cell corrosion

The overall rate of the corrosion process is dependent on the three main partial processes (anodic, cathodic and ohmic) (cf. Figure 1 and Section 1). Their respective influences may be

evaluated by determining the dissipation of energy (potential drop) for each process and relating it to the overall energy loss [12, 31]. This is conceptually illustrated in Figure 10.

In the present research, the energy dissipation arising from the cathodic ($\Delta U_{ct,c}$) and anodic ($\Delta U_{ct,a}$) polarizations was calculated based on Equations (2) and (3), respectively. For the ohmic partial process, it was assumed that $R_{\Omega,c} << R_{\Omega,a}$ and therefore that the energy dissipation through the flow of the macro-cell current in the concrete ($I_{galv} \cdot R_{\Omega}$) is a close approximation of the ohmic drop related to the anode ($I_{galv} \cdot R_{\Omega,a}$). The overall energy dissipation (ΔU) is the sum of all three voltage drops. Relating the potential drops of the partial processes to the overall energy dissipation allows for a quantification of the corrosion rate controlling process (Equations 4 a) – d)).

$$C_{ct,a} = \frac{\Delta U_{ct,a}}{\Delta U} = \frac{R_{pa} \cdot I_{galv}}{\Delta U_{ct,a} + \Delta U_{ct,c} + \Delta U_{\Omega,a}} \quad (4\ a)$$

$$C_{ct,c} = \frac{\Delta U_{ct,c}}{\Delta U} = \frac{\beta_c \log \left| \frac{I_{galv}}{I_c^o} \right|}{\Delta U_{ct,a} + \Delta U_{ct,c} + \Delta U_{\Omega,a}} \quad (4\ b)$$

$$C_{\Omega,a} = \frac{\Delta U_{\Omega,a}}{\Delta U} = \frac{R_{\Omega,a} \cdot I_{galv}}{\Delta U_{ct,a} + \Delta U_{ct,c} + \Delta U_{\Omega,a}} \quad (4\ c)$$

$$C_{\Omega,c} \approx 0 \quad (4\ d)$$

The indices ‘ct’ and ‘Ω’ indicate the nature of the process, i.e. the charge transfer at the steel/concrete interface vs. the ohmic current flow in the electrolyte. Figure 11 depicts the results of this analysis for the present experimental measurements.

Figure 11 shows that the macro-cell corrosion process for the PC specimens (a)) is equally controlled by the cathodic and the anodic process, and virtually independent of the bulk resistivity (in the range 40 – 90 Ωm). For the FA specimens on the other hand, which span a

range of ρ_{bulk} from 400 to 2500 Ωm, the extent to which the cathodic process controls the macro-cell corrosion rate is smaller (roughly 30%). This may be explained by the increase in $R_{\Omega,a}$with the increase in bulk resistivity (Figure 4), and the implications this has for the anodic reaction rate.

As described above, the concept of anodic resistance control combines the charge transfer resistance of the anode ($R_{ct,a}$) and the anodic part of the ohmic partial process ($R_{\Omega,a}$). This is illustrated in Figure 11 with diagonal hatching. From this perspective, the FA specimens are clearly under anodic resistance control, which agrees well with reports by Page and co-workers on mortars/pastes prepared with supplementary cementitious materials [10, 11]. For the PC specimens, this effect is less pronounced, but here too anodic resistance control plays an important role (roughly 50% of the control of the macro-cell corrosion rate).

Although attempts are often made to identify one single rate-limiting step, Figure 11 a) and b) show that the influence of the three partial processes is in most cases comparable. There is no one dominant process that alone limits the corrosion current; it is rather a combination of all three processes. This is in agreement with what other researchers have found (e.g. [25, 27, 28]).

In summary, none of the partial processes can be directly related to the bulk resistivity. Moreover, the corrosion process is controlled by the combined influence of the anodic, cathodic and ohmic partial processes. Consequently, a fundamental correlation cannot be documented between concrete resistivity and the corrosion rate.

4.4 Extrapolating laboratory scale experiments to large-scale structures

In this research, it was considered that the entire cathode surface could contribute to the macro-cell corrosion current. The ohmic resistance of the cathode was neglected because it had earlier been found that the ohmic (spreading) resistance of the anode was considerably higher for the dimensions and cathode-to-anode ratio tested here [21]. However, in large-scale structures, parts of the passive reinforcement steel will be located remote from the anode. Distances of several tens of metres can easily arise. Such remote cathode segments (*i*) will be associated with a high ohmic resistance ($R_{\Omega,c,i}$), which will limit their influence on the corrosion process. On the other hand, the charge transfer resistance of the entire cathode will be very low, because an infinitely large area is available for the cathodic reaction. Since the ohmic resistance of the cathode ($R_{\Omega,c,i}$) is considered a part of the ohmic partial process (cf.Figure9), the corrosion process for large-scale structures with almost infinitely large cathodes can only be under anodic or ohmic control and never under cathodic control. This demonstrates that the rate-limiting step identified in small-scale experiments or for a low cathode-to-anode ratio does not need to correlate to conditions in practice.

5 Conclusions

Experimental investigations were undertaken with instrumented, laboratory-scale mortar specimens in order to study the influence of mortar resistivity on the corrosion kinetics of chloride-induced macro-cell corrosion of steel in concrete. The following conclusions can be drawn:

1) The macro-cell corrosion rate is goverend by a combination of different rate-limiting steps, rather than being solely under anodic, ohmic, or cathodic control. This is in agreement with other results in the literature. Anodic resistance control (covering the

effect of the anodic charge transfer reaction and the ohmic resistance associated with the anode) was found to be the main rate-limiting step influencing the corrosion process, especially for mortar prepared with fly ash.

2) The corrosion kinetics at the anode aregoverned by the local conditions in the close vicinity of the anode. The results indicate mass transfer limitations arising from an inhomogeneous matrix directly influencing the anodic charge transfer reaction.

3) Ohmic resistance arising in the concrete in the direct vicinity of the anode dominates the ohmic partial process for laboratory-scale mortar specimens. The resistance is strongly influenced by local conditions and is therefore not directly correlated to the bulk concrete resistivity.

4) The reaction kinetics of the cathodic partial process (oxygen reduction) depend on the type of concrete and probably on other factors not investigated in this research (saturation state, temperature, cover depth, etc.). It was found that it is not possible to describe the cathodic reaction kinetics as a function of the concrete resistivity.

These four conclusions explain why the correlation between bulk concrete resistivity and the corrosion rate for chloride induced macro-cell corrosion that is frequently claimed in the literature, cannot exist.

Acknowledgements

The paper is based on work carried out at the NTNU, Trondheim and in COIN – the Concrete Innovation Centre (www.coinweb.no) – a centre for research-based innovation, which was

initiated by the Research Council of Norway (RCN) in 2006. The work was also supported by the Norwegian Public Roads Administration (www.vegvesen.no). The 3D scanning was undertaken by Cascade AB, Sweden. The images were analysed by Trine-Lise Lorentsen. Special thanks to Kristian Sætre and Miguel Boix Roca for their help with the experimental work.

References

[1] U. Angst, B. Elsener, C.K. Larsen, Ø. Vennesland, Critical chloride content in reinforced concrete - A review, Cement and Concrete Research, 39 (2009) 1122-1138.

[2] L. Bertolini, B. Elsener, P. Pedeferri, E. Redaelli, R.B. Polder, Corrosion of Steel in Concrete: Prevention, Diagnosis, Repair (2nd Edition), Wiley-VCH Verlag GmbH & Co., 2013.

[3] U. Angst, Chloride induced reinforcement corrosion in concrete - Concept of critical chloride content - methods and mechanisms, Doctoral Thesis, in: Department of Structural Engineering, Norwegian University of Science and Technology, Trondheim, 2011.

[4] J. Gulikers, Experimental investigations on macrocell corrosion in chloride-contaminated concrete, Heron, 41 (1996) 107-123.

[5] G.K. Glass, C.L. Page, N.R. Short, Factors Affecting the Corrosion Rate of Steel in Carbonated Mortars, Corros Sci, 32 (1991) 1283-1294.

[6] A. Tondi, R.B. Polder, R. Cigna, Concrete resistivity and corrosion rate of reinforcement in atmospheric concrete after one year, TNO Building and Construction Research, 1993.

[7] L. Bertolini, R.B. Polder, Concrete resistivity and reinforcement corrosion rate as a function of temperature and humidity of the environment, TNO Building and Construction Research, 1997.

[8] U. Angst, B. Elsener, C.K. Larsen, Ø. Vennesland, Chloride induced reinforcement corrosion: Rate limiting step of early pitting corrosion, Electrochim Acta, 56 (2011) 5877-5889.

[9] S. Jäggi, Experimentelle und numerische Modellierung der lokalen Korrosion von Stahl in Beton unter besonderer Berücksichtigung der Temperaturabhängigkeit (in German), Doctoral Thesis in, ETH, Zürich, 2001.

[10] P. Lambert, C.L. Page, P.R.W. Vassie, Investigations of reinforcement corrosion. 2. Electrochemical monitoring of steel in chloride-contaminated concrete, Mater Struct, 24 (1991) 351-358.

[11] C.L. Page, J. Havdahl, Electrochemical monitoring of corrosion of steel in microsilica cement pastes, Mater Struct, 18 (1985) 41-47.

[12] M. Raupach, Zur chloridinduzierten Makroelementkorrosion von Stahl in Beton (in German), Beuth Verlag GmbH, Berlin, 1992.

[13] Deutscher Ausschuss für Stahlbeton, Dauerhaftigkeitsbemessung von Stahlbetonbauteilen auf Bewehrungskorrosion, Beuth, Berlin, 2012.

[14] J. Warkus, M. Raupach, Numerical modelling of macrocells occurring during corrosion of steel in concrete, Materials and Corrosion, 59 (2008) 122-130.

[15] K. Hornbostel, C.K. Larsen, M.R. Geiker, Relationship between concrete resistivity and corrosion rate - A literature review, Cement Concrete Comp, 39 (2013) 60-72.

[16] L. Bertolini, M. Gastaldi, M.P. Pedeferri, P. Pedeferri, T. Pastore, Effects of galvanic coupling between carbon steel and stainless steel reinforcement in concrete, in: International Conference on Corrosion and Rehabilitation of Reinforced Concrete Structures, Orlando, USA, 1998.

[17] K. Hornbostel, The role of concrete resistivity in chloride-induced macro-cell corrosion of reinforcement, Doctoral Thesis (submitted), in: Department of Structural Engineering, Norwegian University of Science and Technology (NTNU), Trondheim, Norway, 2015.

[18] S. Jäggi, B. Elsener, H. Bohni, Oxygen reduction on mild steel and stainless steel in alkaline solutions, European Federation of Corrosion Publications, 31 (2000) 3-12.

[19] U.M. Angst, B. Elsener, C.K. Larsen, O. Vennesland, Chloride induced reinforcement corrosion: Electrochemical monitoring of initiation stage and chloride threshold values, Corros Sci, 53 (2011) 1451-1464.

[20] P.V. Nygaard, M.R. Geiker, A method for measuring the chloride threshold level required to initiate reinforcement corrosion in concrete, Mater Struct, 38 (2005) 489-494.

[21] K. Hornbostel, U. Angst, B. Elsener, C.K. Larsen, M.R. Geiker, On the limitations of predicting the ohmic resistance in a macro-cell in mortar from bulk resistivity measurements, Cement & Concrete Research 76 (2015) 147-158.
[22] W. Oelssner, F. Berthold, U. Guth, The iR drop - well-known but often underestimated in electrochemical polarization measurements and corrosion testing, Mater Corros, 57 (2006) 455-466.
[23] H.R. Copson, The electrochemical nature of corrosion, in: F.L. LaQue, H.R. Copson (Eds.) Corrosion resistance of metals and alloys, Reinhold Publishing Corporation, New York, 1963, pp. 83-105.
[24] M.F. Beck, Zur Entwicklung der Eigenkorrosion von Stahl in Beton (in German), Doctoral Thesis, in, RWTH Aachen, 2010.
[25] J. Warkus, Einfluss der Bauteilgeometrie auf die Korrosionsgeschwindigkeit von Stahl in Beton bei Makroelementbildung, Deutscher Ausschuss für Stahlbeton, Beuth, Berlin, 2014.
[26] U. Nürnberger, Korrosion und Korrosionsschutz im Bauwesen, Bauverlage, Wiesbaden and Berlin, 1995.
[27] M. Brem, Numerische Modellierung der Korrosion in Stahlbetonbauten Anwendung der Boundary Element Methode (in German), Doctoral Thesis, in, Zürich, 2004, pp. 174 S.
[28] J. Nöggerath, Makroelementkorrosion von Stahl in Beton - Wirkungsweise und Einflussgrößen (in German), Doctoral Thesis, in: Insitut für Baustoffe, Werkstoffchemie und Korrosion, ETH Zurich, Zurich, Switzerland, 1990.
[29] J. Warkus, M. Raupach, Modelling of reinforcement corrosion - geometrical effects on macrocell corrosion, Materials and Corrosion, 61 (2010) 494-504.
[30] H. Kaesche, Corrosion of metals - Physicochemical principles and current problems Springer Science & Business Media, Berlin u.a., 2003.
[31] M. Raupach, J. Gulikers, Investigations on cathodic control of chloride-induced reinforcement corrosion, Mater Corros, 52 (2001) 766-770.

Table 1 – List of symbols and abbreviations.

Symbol	Unit	Explanation
AP	-	Anodic polarization curve
CP	-	Cathodic polarization curve
E_a	[mV]	Anode potential
E_a^{rev}	[mV]	Reversible anode potential
E_c	[mV]	Cathode potential
E_c^{rev}	[mV]	Reversible cathode potential
FA	-	Mortar with Portland cement and fly ash
I^o/ i^o	[μA] / [μA/cm^2]	Exchange current / Exchange current density
I_{corr} / i_{corr}	[μA] / [μA/cm^2]	Corrosion current / Corrosion rate
I_{galv}	[μA]	Galvanic current
k	[m]	Cell constant
PC	-	Mortar with Portland cement
$R_{ct,a}$	[Ω]	Charge transfer resistance anode
$R_{ct,c}$	[Ω]	Charge transfer resistance cathode
R_{pa}	[Ω] / [Ωm^2]	Polarization resistance of the simulated anode
$R_{\Omega,a}$	[Ω]	Anodic part of the ohmic partial process (here: resistance between simulated anode and cathode network)
$R_{\Omega,c}$	[Ω]	Cathodic part of the ohmic partial process
SCE	-	Saturated calomel electrode
w/b	[-]	Water/binder ratio
β_c	[V/decade]	Cathodic Tafel slope
ΔU	[V]	Total energy dissipation / driving voltage of the macro-cell
$\Delta U_{ct,a}$	[V]	Energy dissipation/ voltage drop of the anodic partial process
$\Delta U_{ct,c}$	[V]	Energy dissipation/ voltage drop of the cathodic partial process
$\Delta U_{\Omega,a}$	[V]	Energy dissipation/ voltage drop of the anodic part of the ohmic partial process
ρ_{bulk}	[Ω·m]	Bulk mortar resistivity

Table 2 – Mortar composition and properties.

a) Mortar composition

Composition		PC	FA
Cement (CEM I 42.5 R)*1	[kg/m3]	503.2	378.4
Silica fume (920 D)	[wt. %/cement]		6
Fly ash	[wt. %/cement]		45.6
Water/binder*2	[-]	0.55	0.4
Aggregate (0-4)	[wt. %/aggregate]	80	100
Aggregate (0-2)	[wt. %/aggregate]	20	
Superplasticizer (SP130)*3	[wt. %/cement]		1.2
Paste	[l/m3]	438	438

*1 Norcem
*2 efficiency factor = 1
*3 Mapei

b) Mortar properties

Property		PC	FA
Slump	[mm]	140	250
Density	[kg/m3]	2196	2212
Air content	[%]	5	3.5
Compressive strength at 28 days	[MPa]	45	58

Table 3 – Exposure conditions and specimen IDs.

a) PC specimens (3 specimens per series)

	Specimen ID			Age [weeks]													
	PC5D	PC20D	PC35D														
	Temperature			1	2	3	4	5-8	9	10-17	18-43	44	45-53	54-91	92	93	94-…
Casting		20°C															
Curing (sealed, climate room)		20°C															
Epoxy coating + cutting of the cover		20°C															
Drying (oven)		30°C															
Storage (laboratory)		20°C															
Exposure to 3mol NaCl solution	5°C	20°C	35°C														
Stored in closed boxes (RH~85%)	5°C	20°C	35°C														
Stored in closed boxes (RH~85%)		20°C															
Storage (laboratory)		20°C															
Stored in closed boxes (RH~30%)		20°C															
Exposure to tap water		20°C															
Stored in closed boxes (RH~85%)	5°C	20°C	35°C														
Storage (laboratory)		20°C															
Measurement presented in the paper											x			x	x	x	x

b) FA specimens (3 specimens per series)

	Specimen ID			Age [weeks]											
	FA5D	FA20D	FA35D												
	Temperature			1	2-19	20	21-23	24	25	26-54	55-87	88-92	93	94	95-…
Casting		20 °C													
Curing (sealed, 20 °C, climate room)		20 °C													
Epoxy coating + cutting of the cover		20 °C													
Drying (oven)		30 °C													
Storage (laboratory)		20 °C													
Exposure to 3mol NaCl solution	5 °C	20 °C	35°C												
Stored in closed boxes (RH~85%)	5 °C	20 °C	35°C												
Stored in closed boxes (RH~85%)		20 °C													
Storage (laboratory)		20 °C													
Exposure to 3mol NaCl solution		20 °C													
Stored in closed boxes (RH~85%)	5 °C	20 °C	35°C												
Storage (laboratory)		20 °C													
Measurement presented in the paper										x		x	x	x	x

Table 4 – Volume loss determined from 3D scanning and calculated on the basis of galvanic current measurements for Portland cement (PC) specimens (~ 86 weeks after corrosion initiation) and for fly ash (FA) specimens (~71 weeks after corrosion initiation).

Specimen	Volume loss from I_{galv} measurements (V_{galv}) [mm^3]	Volume loss from 3D scanning (V_{3D}) [mm^3]	Micro-cell corrosion (V_{3D} - V_{galv}) [mm^3]
PC5D1	17.8	/	
PC5D2	18.3	12.0	-6.3 (-52%)
PC5D3	13.3	/	
PC20D1	22.8	20.1	-2.7 (-13%)
PC20D2	19.6	/	
PC20D3	26.2	/	
PC35D1	24.9	/	
PC35D2	23.4	23.2	-0.2 (-1%)
PC35D3	38.3	40.6	2.3 (6%)
FA5D1	/*	/	
FA5D2	/*	/	
FA5D3	3.0	8.0	5.0 (63%)
FA20D1	2.3	6.0	3.7 (62%)
FA20D2	2.0	/	
FA20D3	1.7	/	
FA35D1	2.6	4.9	2.3 (47%)
FA35D2	1.9	/	
FA35D3	1.5	6.5	5.0 (77%)

* These specimens were excluded from the analyses due to a short circuit found between the anode and cathode

Figure 1 – Process of chloride-induced reinforcement corrosion, after [2, 3].

Figure 2 – Sketch of the mortar specimens, position as cast and tested (measurements in mm). The initial cover of 30 mm was reduced to 10 mm by cutting after curing to facilitate exposure to chlorides from the lower side.

Figure 3 – 3D scans of two corroded simulated anodes.

Figure 4 – Comparison between $R_{\Omega,a}$ (see explanation in the text) and the bulk resistivity.

Figure 5 – Examples of representative polarization curves (compensated for IR drop): a) Potentials vs. current and b) Potentials vs. logarithm of current, (specimen FA35D1, 95 weeks after casting).

Figure 6 – Comparison between the cathodic polarization behaviour and the bulk resistivity.

Figure 7 – Comparison between the polarization resistance of the simulated anodes and a) the bulk resistivity and b) $R_{\Omega,a}$ (see explanation in the text). The polarization resistance of the anode was normalized to the exposed area of the simulated anode (second Y-axes in the figures).

Figure 8 – Comparison between the galvanic current and a) the bulk resistivity and b) $R_{\Omega,a}$ (see explanation in the text). The dashed grey line indicates the position of the overall trend for the data of the FA specimens taking into account an increase in the corrosion current due to self-corrosion (~50%) – see also explanations in the text.

Figure 9 – Simplified circuit equivalent to the macro-cell corrosion process. Indicated are the concepts of anodic resistance control (diagonal hatching) and the difference between small and large-scale samples (see explanations in relevant sections).

Figure 10 – Simplified schematic illustration of the energy dissipation during the corrosion process, shown in a potential vs. log current diagram for small-scale experiments ($\Delta U_{\Omega,c} \sim 0$).

Figure 11 – Rate-limiting step of the macro-cell corrosion process (see explanations in the text and cf. Figure 10).

Figure 1
Click here to download high resolution image

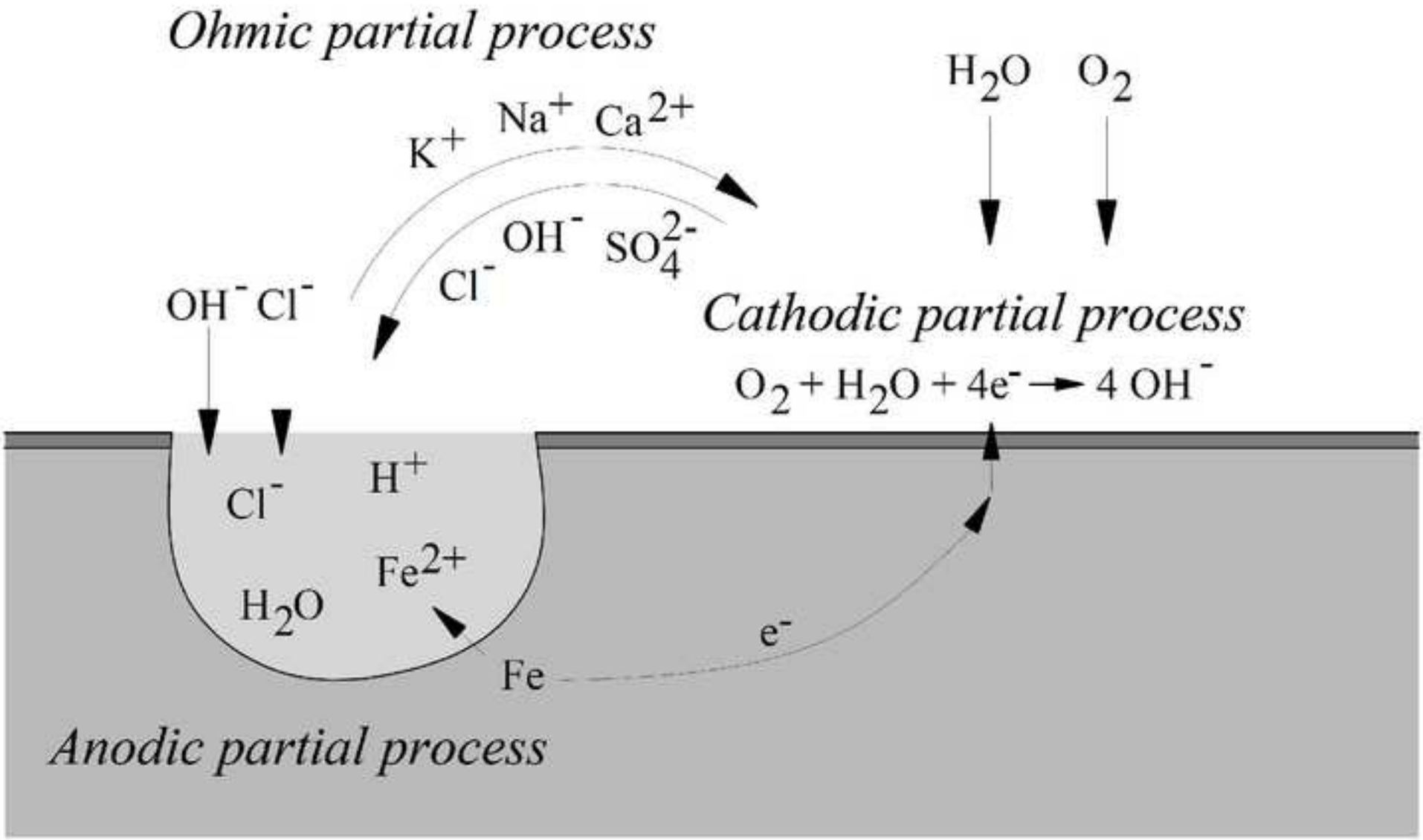

Figure 2
Click here to download high resolution image

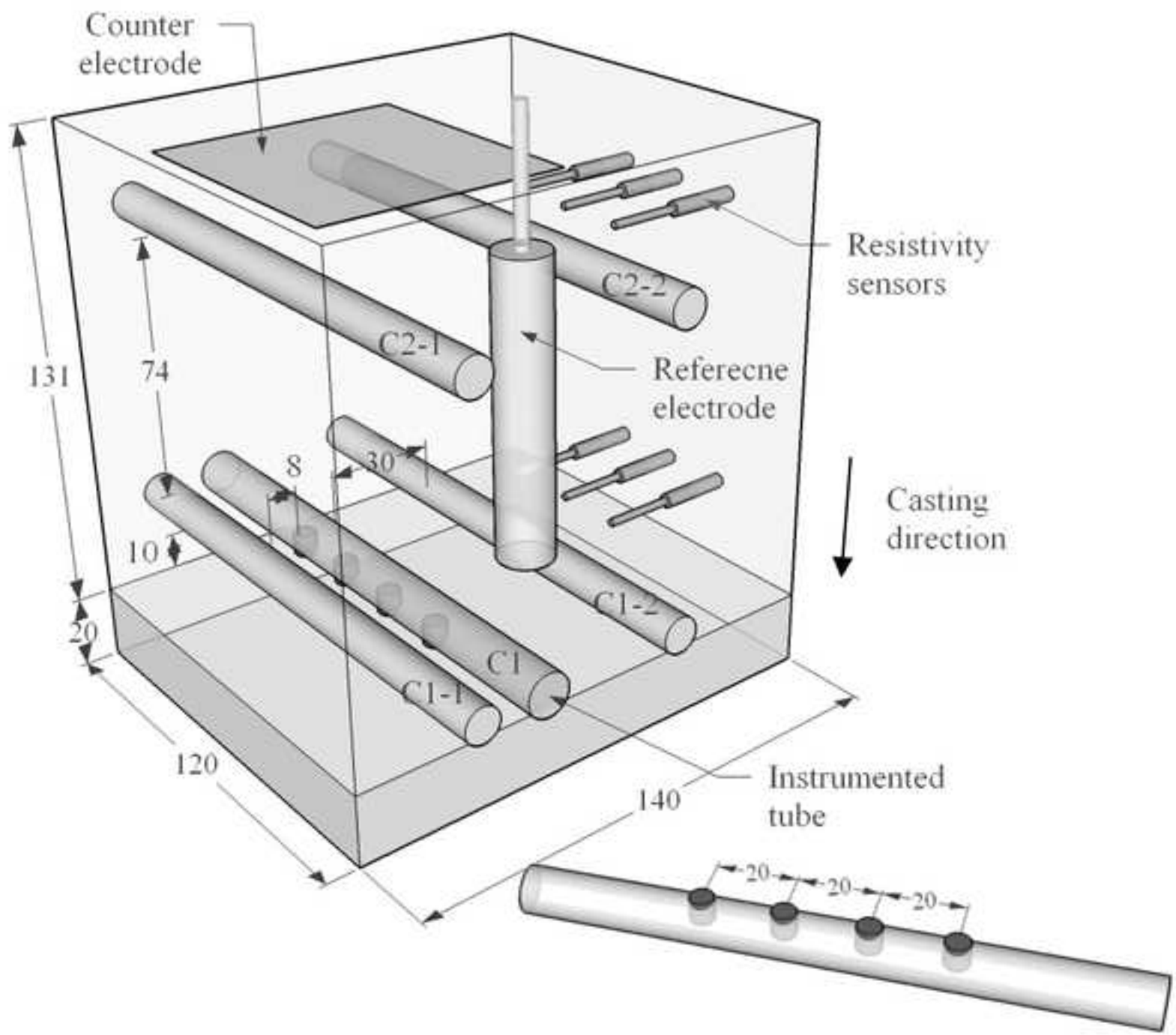

Figure 3a
Click here to download high resolution image

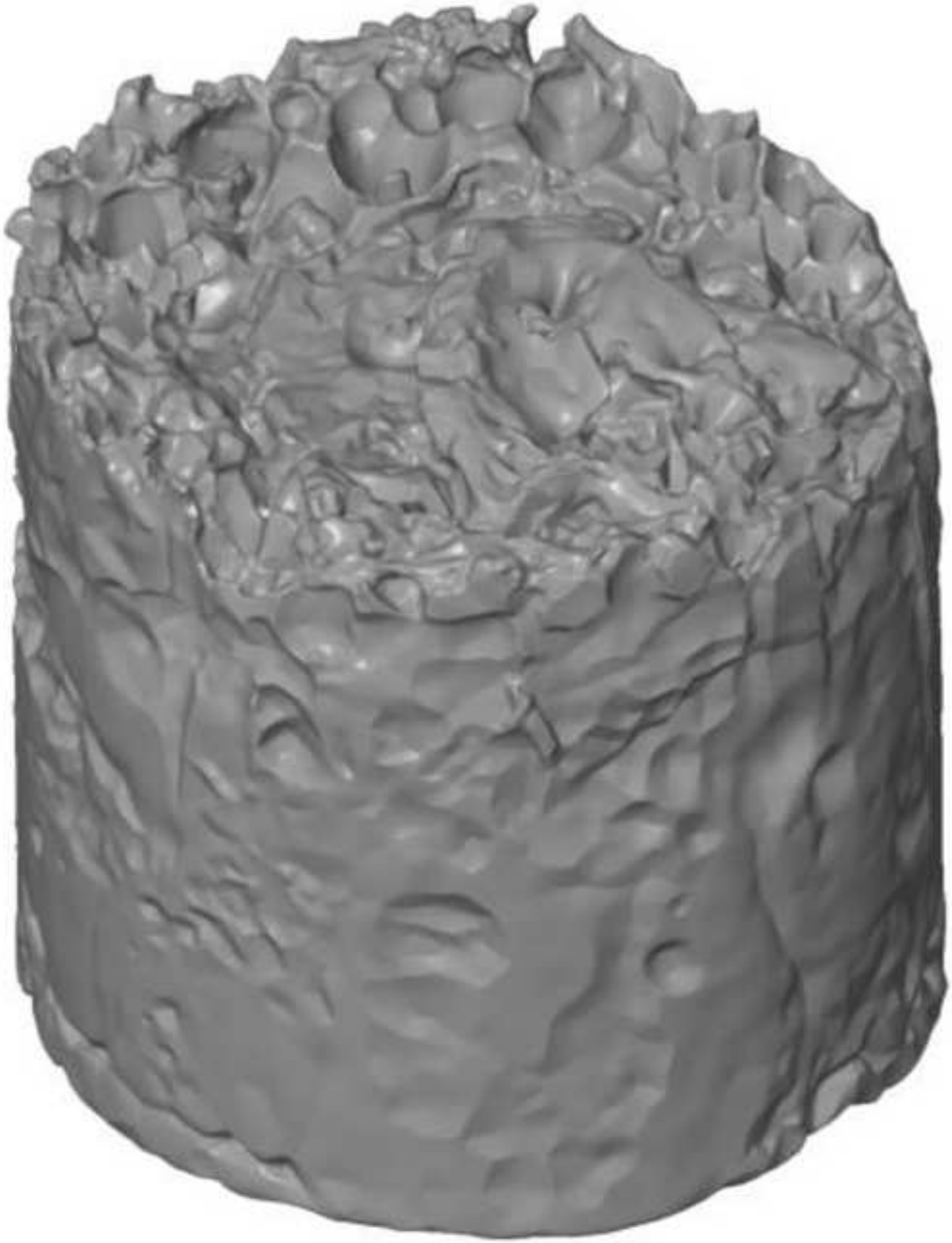

Figure 3b

Click here to download high resolution image

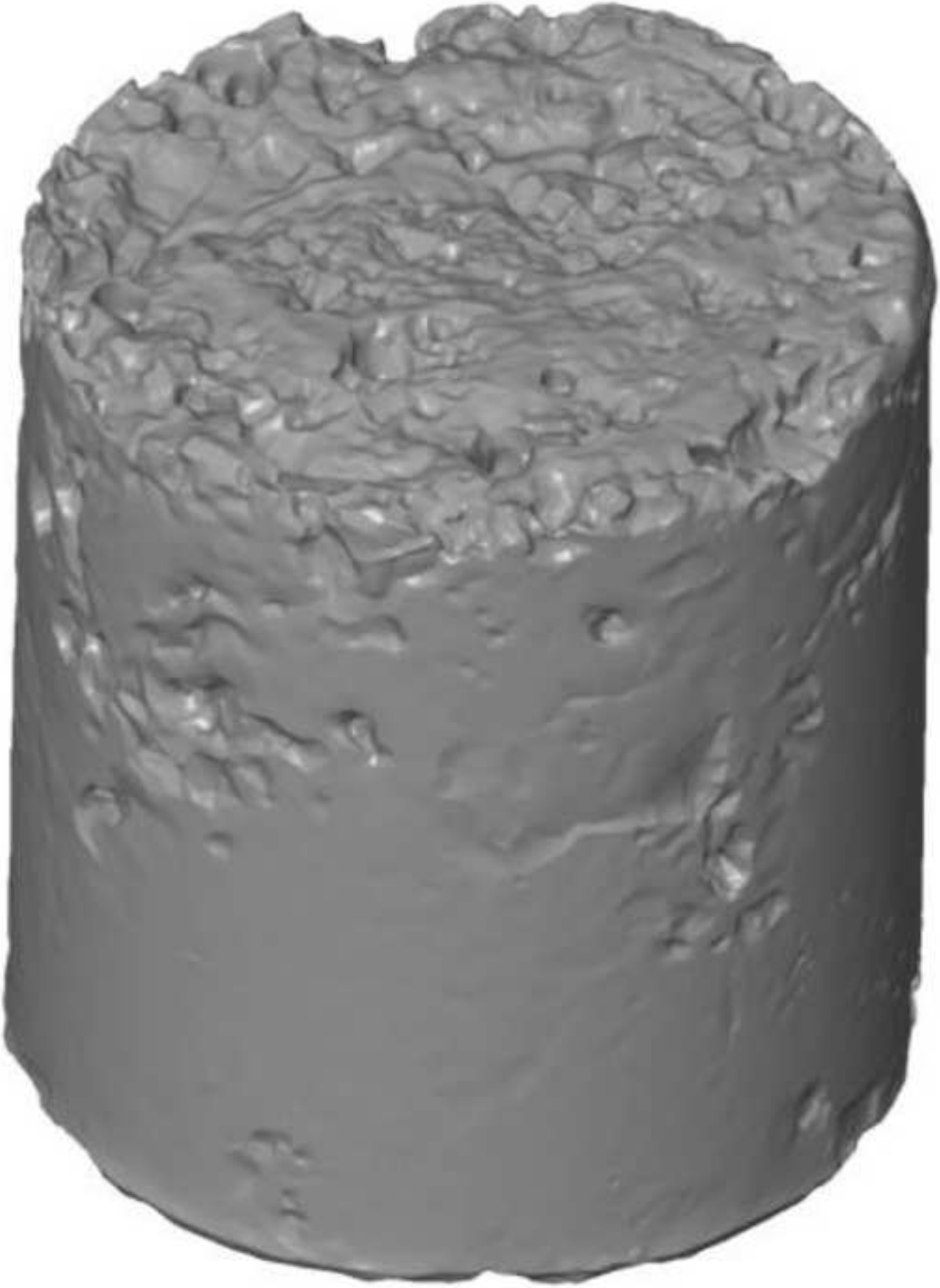

Figure 4
Click here to download high resolution image

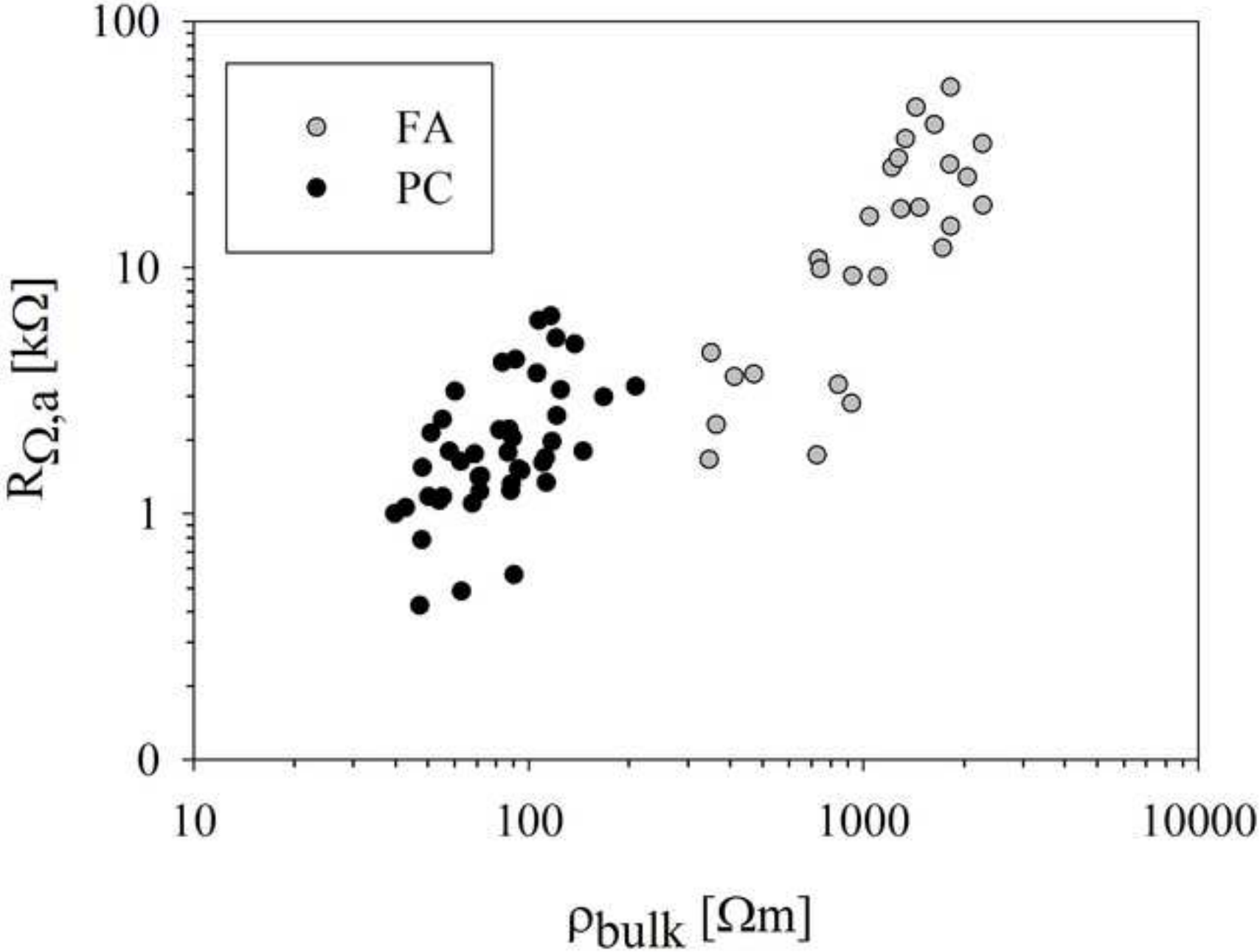

Figure 5a
Click here to download high resolution image

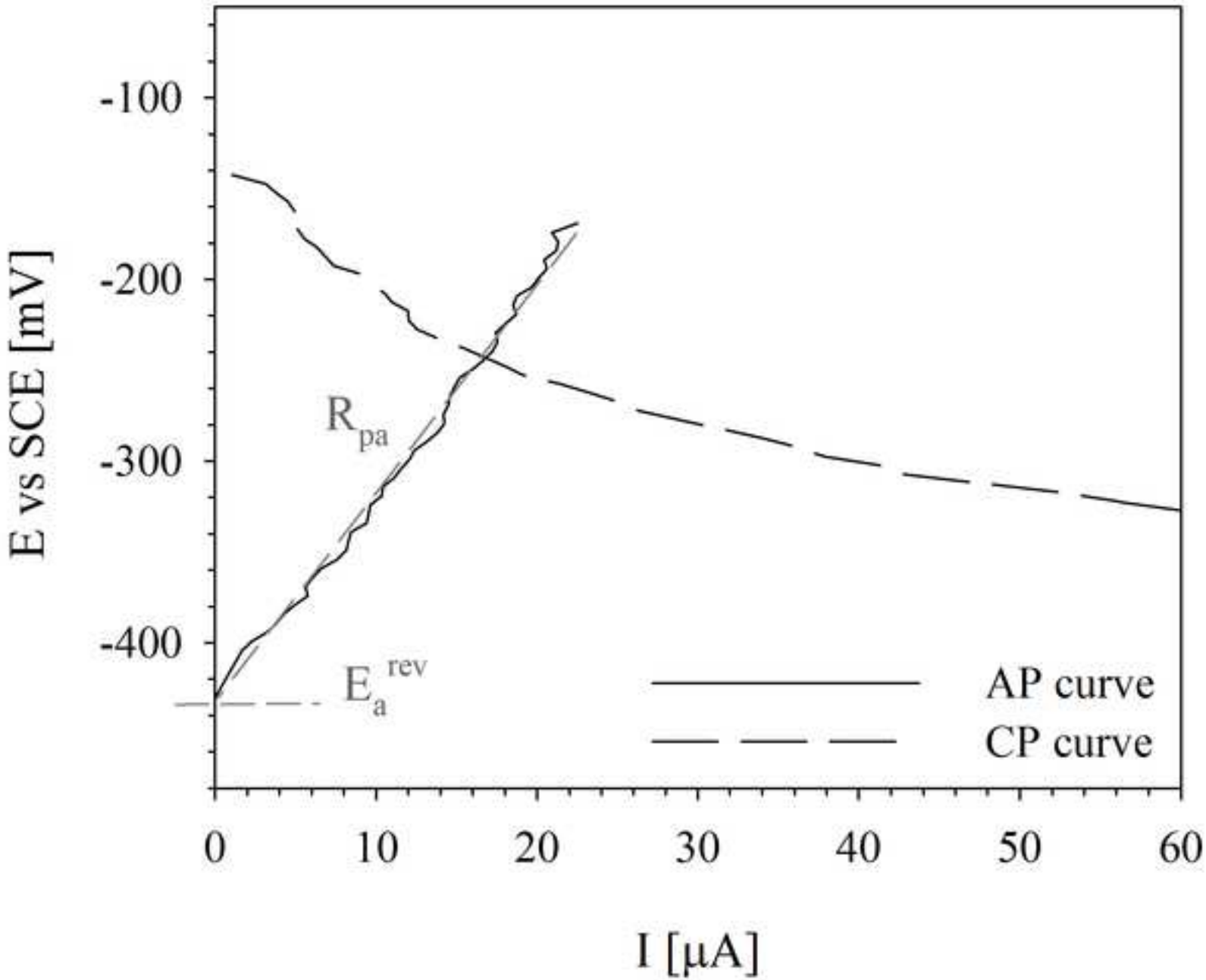

Figure 5b
Click here to download high resolution image

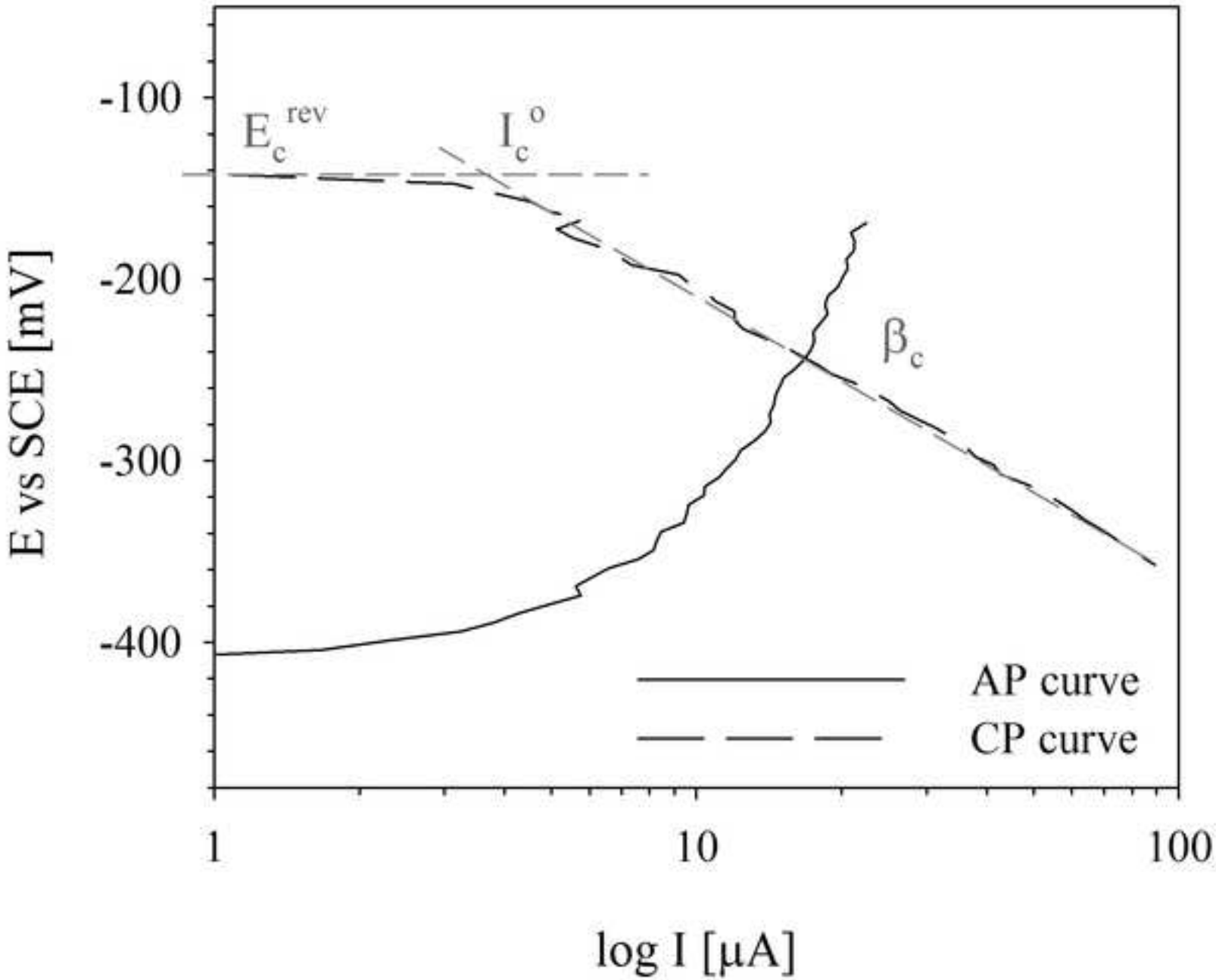

Figure 6a
Click here to download high resolution image

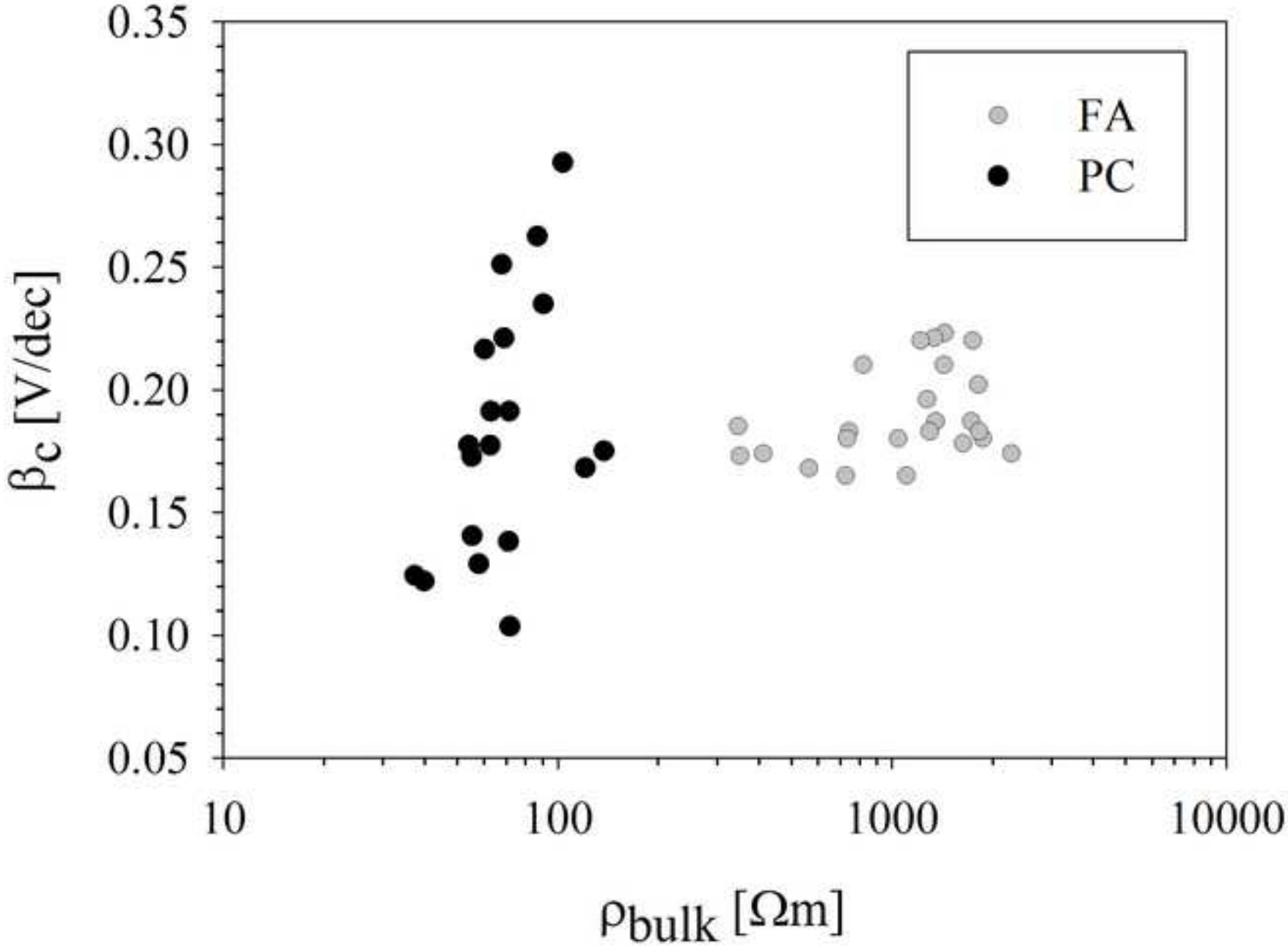

Figure 6b
Click here to download high resolution image

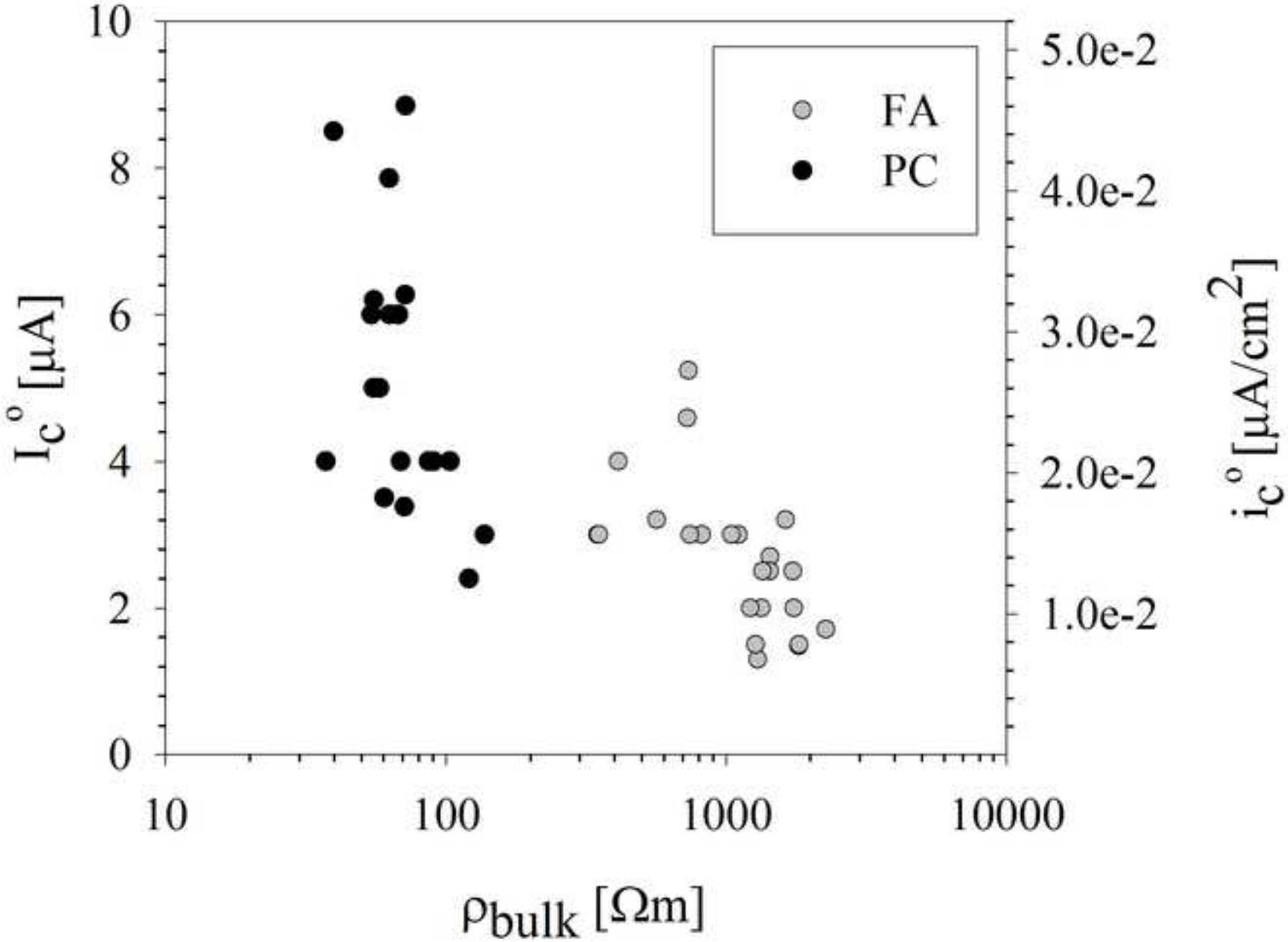

Figure 7a
Click here to download high resolution image

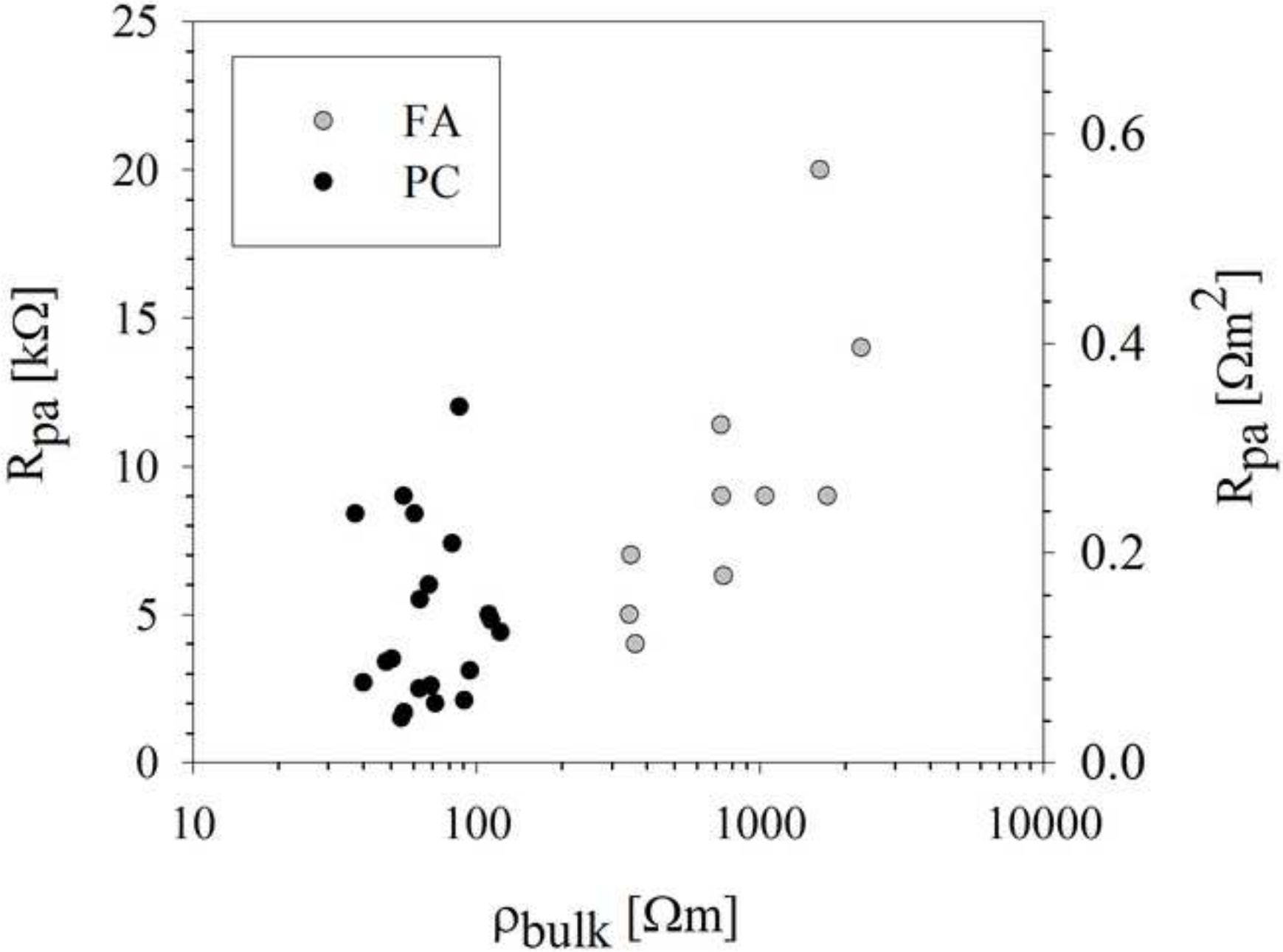

Figure 7b
Click here to download high resolution image

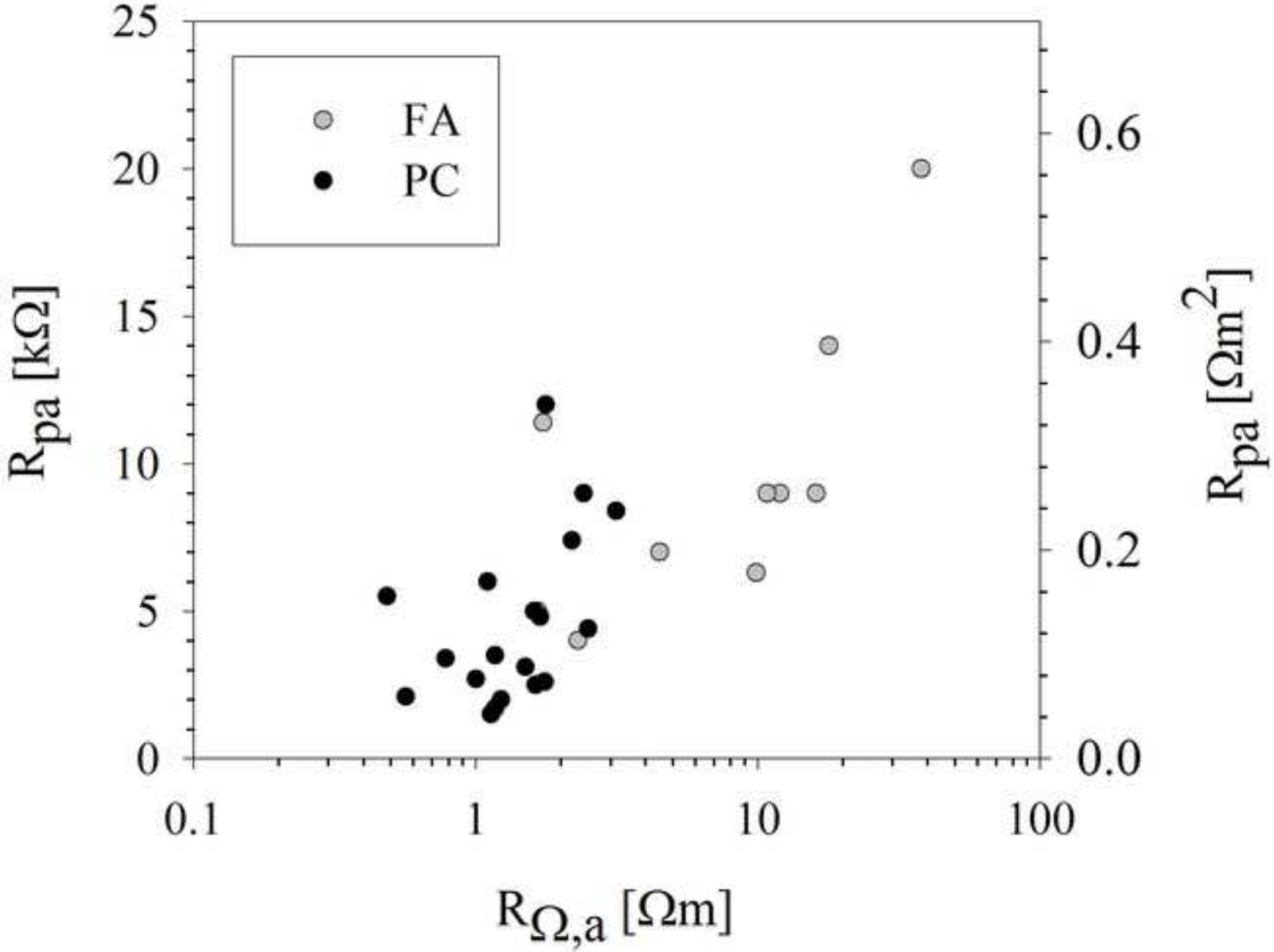

Figure 8a
Click here to download high resolution image

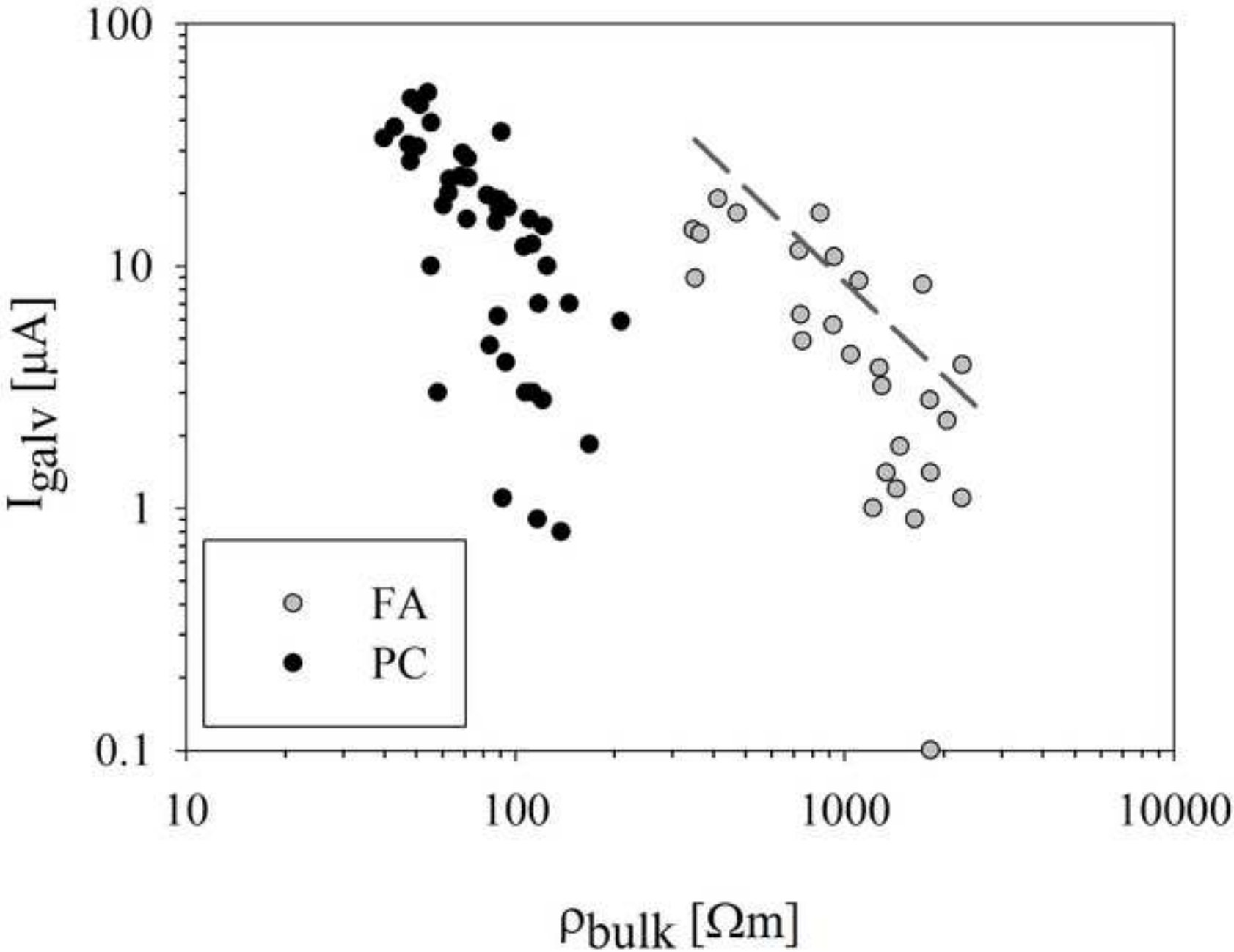

Figure 8b
Click here to download high resolution image

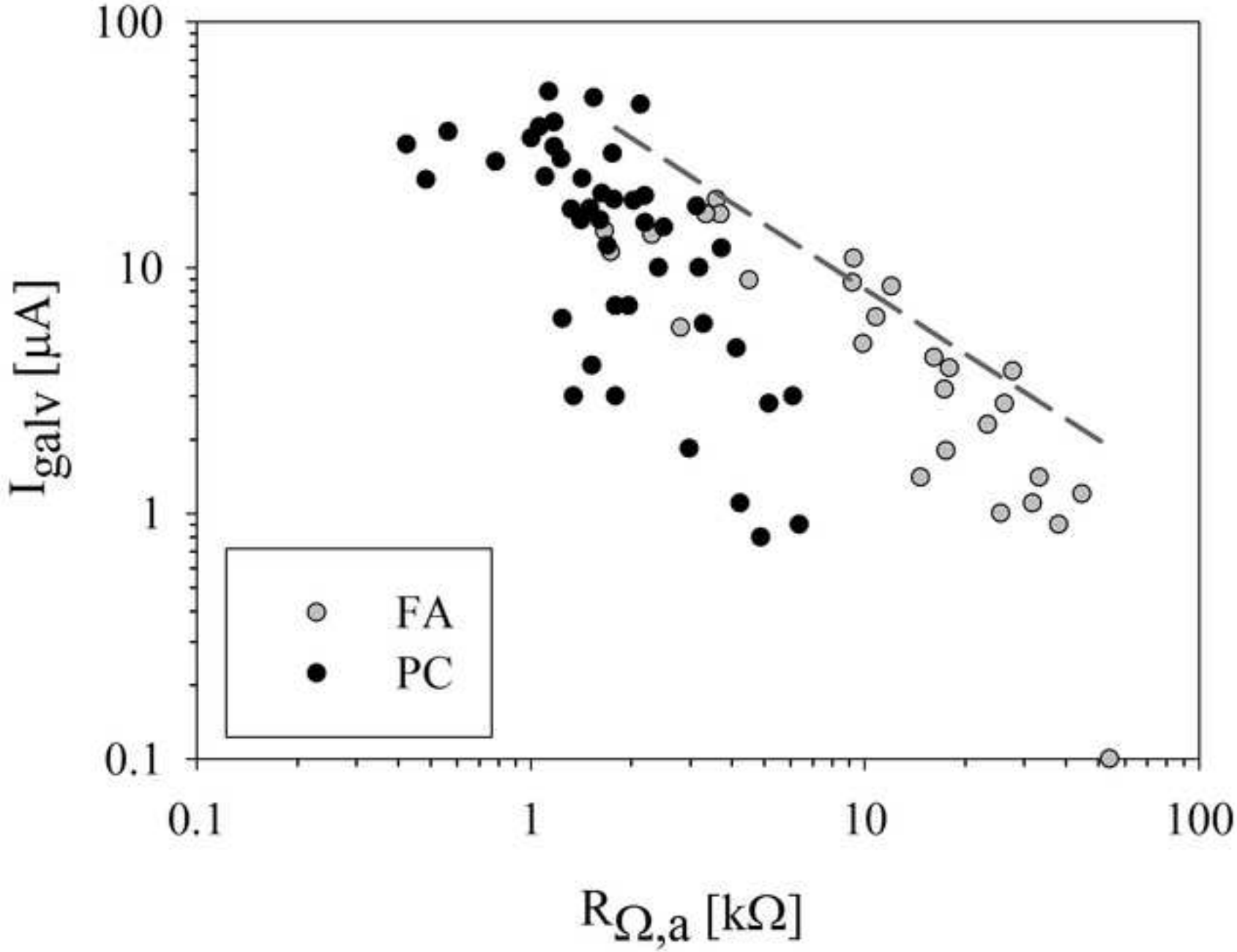

Figure 9
Click here to download high resolution image

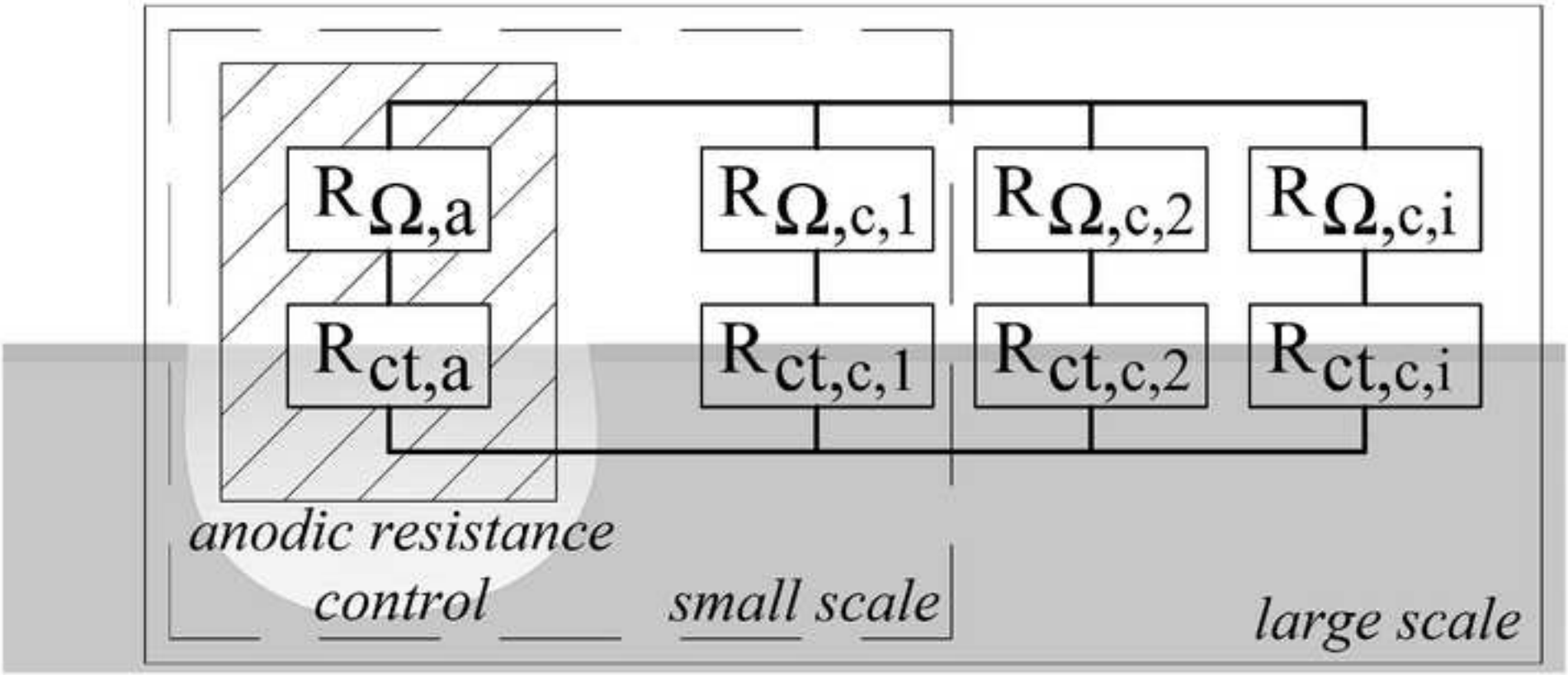

Figure 10
Click here to download high resolution image

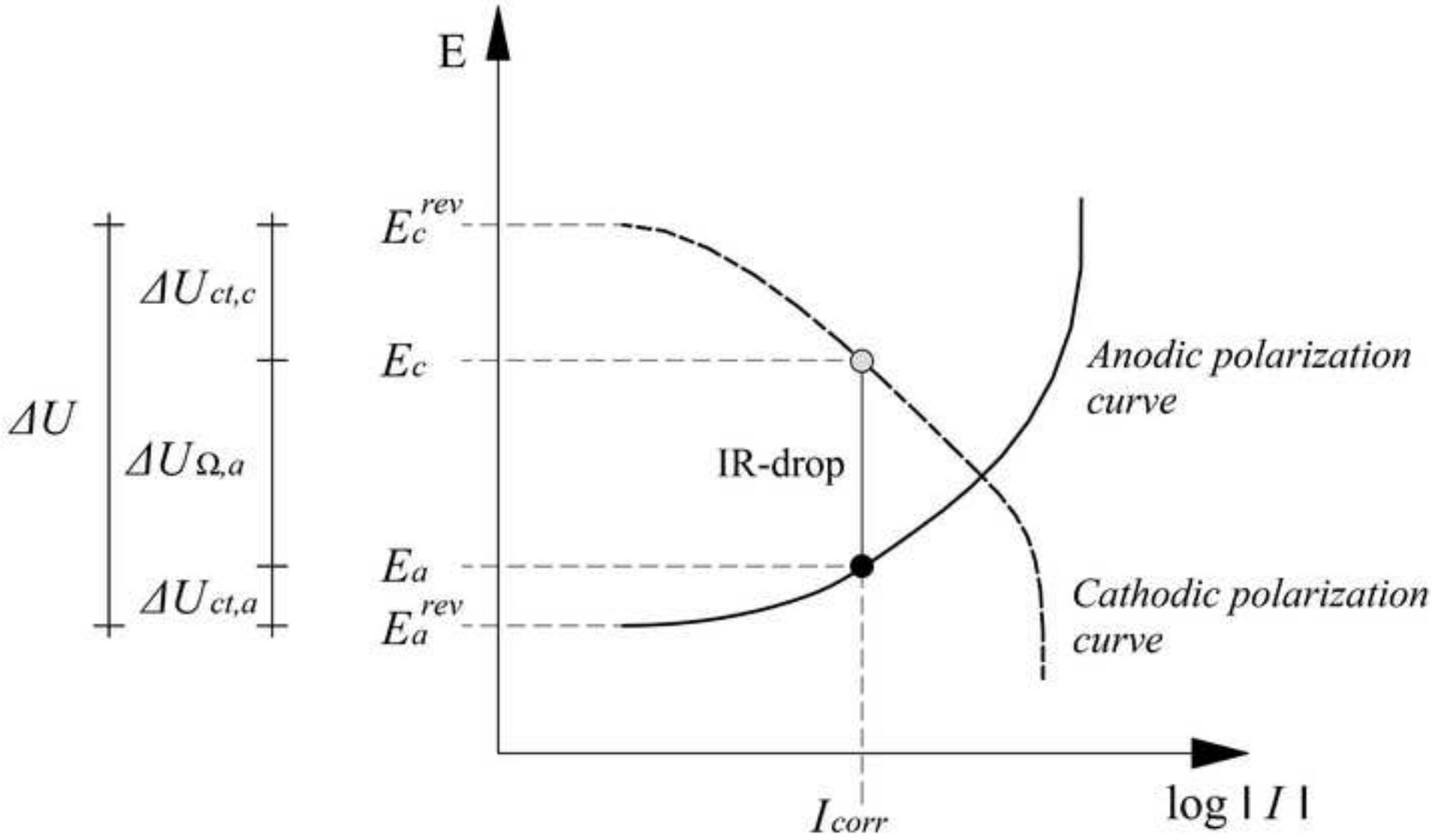

Figure 11a
Click here to download high resolution image

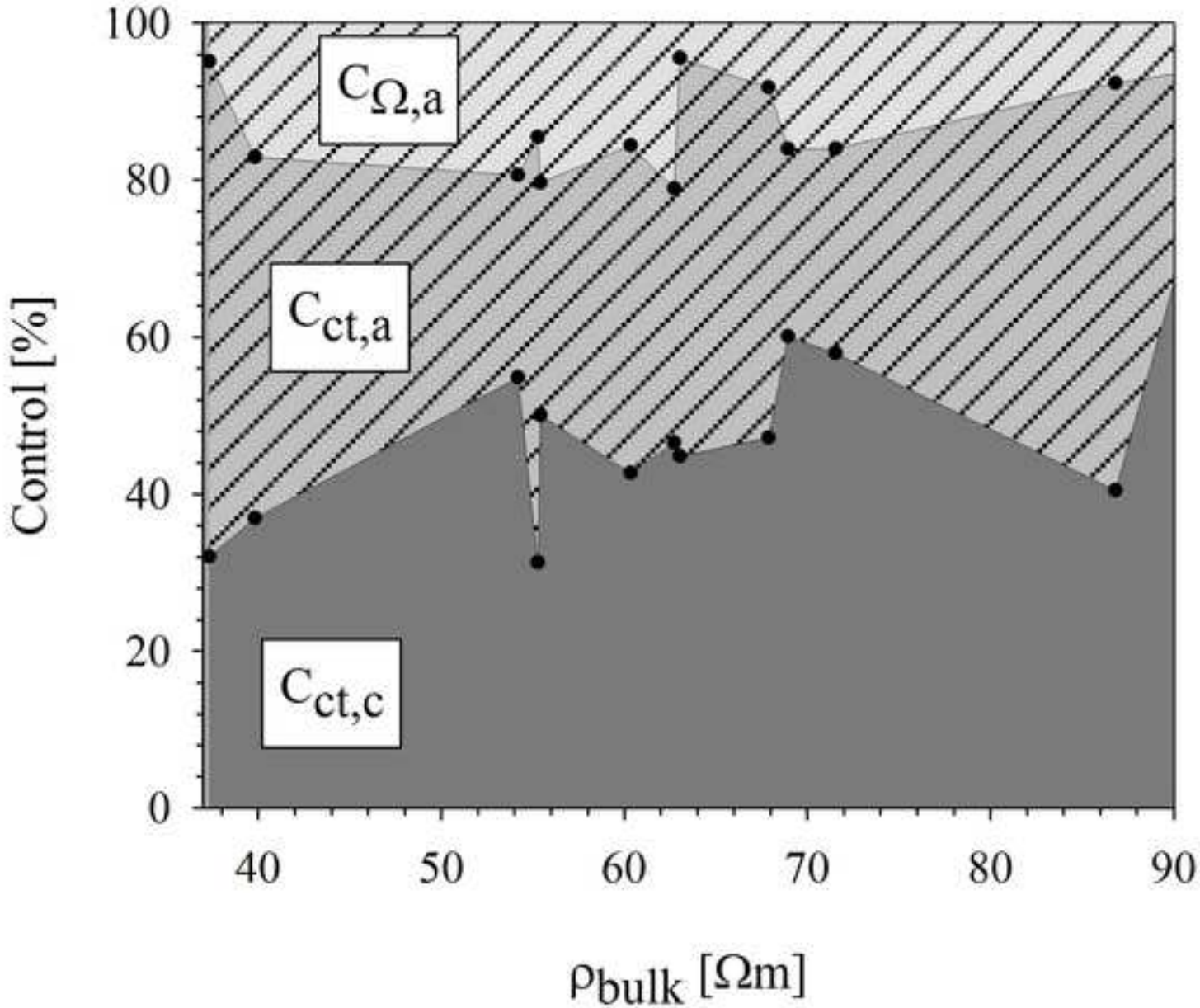

Figure 11b
Click here to download high resolution image